Network localization of cervical dystonia based on causal brain lesions

Daniel T. Corp,*[1,2] Juho Joutsa,*[1,3,4,5] R. Ryan Darby,[1,6] Cathérine C. S. Delnooz[7], Bart P. C. van de Warrenburg[8], Danielle Cooke[1], Cecília N. Prudente[9], Jianxun Ren[3], Martin M. Reich[1,10], Amit Batla[11], Kailash P. Bhatia[12], H.A. Jinnah[13], Hesheng Liu[3], and Michael D. Fox[1,3,14]

[1]Berenson-Allen Center for Non-Invasive Brain Stimulation and Division of Cognitive Neurology, Department of Neurology, Beth Israel Deaconess Medical Center, Harvard Medical School, Boston, MA 02215, USA
[2]Cognitive Neuroscience Unit, School of Psychology, Deakin University, 221 Burwood Highway, Burwood, VIC 3125, Australia
[3]Athinoula A. Martinos Center for Biomedical Imaging, Massachusetts General Hospital and Harvard Medical School, Charlestown, MA 02129, USA
[4]Department of Neurology, University of Turku, Turku, Finland
[5]Division of Clinical Neurosciences, Turku University Hospital, Turku, Finland
[6]Department of Neurology, Division of Cognitive and Behavioral Neurology, Vanderbilt University Medical Center, Nashville, TN, 37232
[7]Department of Neurology, Máxima Medical Centre, Veldhoven, The Netherlands
[8]Department of Neurology, Donders Institute for Brain, Cognition, and Behaviour, Radboud University Medical Centre, Nijmegen, The Netherlands
[9]MicroTransponder, Austin, TX 78738, USA
[10]Deparment of Neurology, University Hospital and Julius-Maximilians-University, Wuerzburg, Germany
[11]UCL Institute of Neurology, Queen Square, London, WC1N 3BG, UK
[12]Sobell Department of Movement Neuroscience, Institute of Neurology, UCL, National Hospital for Neurology, Queen Square, London, WC1N 3BG, UK
[13]Department of Neurology, Emory University, Atlanta, Georgia
[14]Department of Neurology, Massachusetts General Hospital, Harvard Medical School, Boston, MA 02114, USA

*Equal contribution

Correspondence to: Daniel T. Corp (danieltcorp@gmail.com) or Michael D. Fox (foxmdphd@gmail.com)
Running title: Brain network of cervical dystonia

Abstract

Cervical dystonia is a neurological disorder characterized by sustained, involuntary movements of the head and neck. Most cases of cervical dystonia are idiopathic, with no obvious cause, yet some cases are acquired, secondary to focal brain lesions. These latter cases are valuable as they establish a causal link between neuroanatomy and resultant symptoms, lending insight into the brain regions causing cervical dystonia and possible treatment targets. However, lesions causing cervical dystonia occur in multiple different brain locations, leaving localization unclear. Here, we employ a technique termed 'lesion network mapping' which uses connectome data from a large cohort of healthy subjects (resting state fMRI, N = 1000) to test whether lesion locations causing cervical dystonia map to a common brain network. We then test whether this network, derived from brain lesions, is abnormal in patients with idiopathic cervical dystonia (N = 39) versus matched controls (N = 37). A systematic literature search identified 25 cases of lesion-induced cervical dystonia. Lesion locations were heterogeneous, with lesions scattered throughout the cerebellum, brainstem, and basal ganglia. However, these heterogeneous lesion locations were all part of a single functionally connected brain network. Positive connectivity to the cerebellum and negative connectivity to the somatosensory cortex were specific markers for cervical dystonia compared to lesions causing other neurological symptoms. Connectivity with these two regions defined a single brain network that encompassed the heterogeneous lesion locations causing cervical dystonia. These cerebellar and somatosensory regions also showed abnormal connectivity in patients with idiopathic cervical dystonia. Finally, the most effective deep brain stimulation sites for treating dystonia were connected to these same cerebellar and somatosensory regions identified using lesion network mapping. These results lend insight into the causal neuroanatomical substrate of cervical dystonia, demonstrate convergence across idiopathic and acquired dystonia, and identify a network target for dystonia treatment.

Keywords

Cervical dystonia, lesions, functional connectivity, cerebellum, somatosensory cortex

Introduction

Cervical dystonia (CD) is a chronic neurological disorder characterized by sustained and involuntary contractions of the neck muscles, and is the most common form of focal dystonia (Xiao et al., 2012). CD has traditionally been ascribed to dysfunction of the basal ganglia (Galardi et al., 1996; Naumann et al., 1998), but abnormalities have been observed in many other brain regions including the cerebellum (Batla et al., 2015), prefrontal cortex (Li et al., 2017), midbrain (Holmes et al., 2012), motor cortex (Richardson, 2015), and somatosensory cortex (Prudente et al., 2016). This has led to the suggestion that CD is a 'network disorder' resulting from dysfunction in multiple different brain regions (Jinnah et al., 2006). However, the key nodes of this network have yet to be identified. Further, it remains unclear which brain regions are causative and which are compensatory or incidental correlates.

Occasionally, a focal brain lesion can cause symptoms that are nearly identical to those observed in idiopathic CD (LeDoux et al., 2003; Albanese et al., 2013). Although these cases of acquired CD are rare compared to cases of idiopathic CD, they are uniquely valuable because lesions allow for causal links between the damaged brain region and resultant symptoms (Adolphs, 2016; Fox, 2018). However, lesions causing CD can occur in numerous brain locations, spanning the cerebellum, medulla, pons, midbrain, and basal ganglia (LeDoux et al., 2003). Further, symptoms can emerge not only from the lesion itself, but also from the effect of the lesion on remote but connected brain regions, a phenomenon referred to as diaschisis (von Monakow, 1914; Carrera et al., 2014). These factors complicate the localization of CD symptoms based on focal brain lesions alone.

Recently, we validated a technique termed 'lesion network mapping', which can link lesions in different locations to a common brain network (Boes et al., 2015). Rather than focusing solely on lesion location, this technique uses a database of normative resting state functional connectivity MRI (rs-fcMRI) scans to identify the network of brain regions connected to each lesion location. This technique has lent insight into the localization of multiple neuropsychiatric symptoms (Fox, 2018), including other movement disorders (Fasano et al., 2016; Laganiere et al., 2016; Joutsa et al., 2018a), and may help identify therapeutic targets for brain stimulation therapies (Joutsa et al.,

2018a; Joutsa et al., 2018b). Here, we apply this approach to lesions causing CD. We then go beyond prior lesion network mapping studies by investigating whether the neuroanatomical substrate of CD derived from focal brain lesions is also abnormal in patients with similar symptoms, but without brain lesions.

Materials and methods

Case selection

Cases of lesions causing CD were identified from a systematic search of Pubmed in January 2017 using the combination of synonyms of the following terms: cervical dystonia; torticollis; lesion; infarct; tumor; magnetic resonance imaging; and computerized tomography. The exact search syntax is provided in the Supplementary methods. Reference lists of selected articles were searched for possible cases missed in the initial search. Inclusion criteria were: 1) neurological examination documenting CD that was thought to be caused by an intraparenchymal brain lesion(s); 2) a figure or image showing the lesion location in sufficient clarity for it to be traced onto a standard brain atlas. Exclusion criteria were: 1) lesions in children aged <10, given that in these cases the brain is not sufficiently developed to resemble the standard adult brain; 2) lesions of the central nervous system but outside the brain (e.g. meningioma). As the emergence of dystonia may be delayed by months or even years following a brain insult (Scott et al., 1996; LeDoux et al., 2003), we did not apply a strict time limit for the onset of symptoms post-lesion. Based on these criteria, it's important to note that not all lesions causing CD found in our search, which would be eligible for clinical description (e.g. LeDoux & Brady, 2003), were eligible for inclusion in the current analysis.

Lesion network mapping

The network of regions functionally connected to each lesion location was identified using previously described methods (Boes et al., 2015; Darby et al., 2018a). First, lesions from published images were traced by hand onto a standardized brain atlas (2x2x2mm MNI 152 brain) using FSL software (version 5.0.9) (Jenkinson et al., 2012). This approach generates only 2D slices of 3D lesions, but prior work has shown that the resulting connectivity maps are nearly identical (Boes et al., 2015; Darby et al., 2018a). Second, rs-fcMRI maps were created for each lesion using a

standard seed-based approach, leveraging rs-fcMRI data from a normative dataset of 1000 healthy young adults (Yeo et al., 2011; Holmes et al., 2015). The time course of the average blood oxygen level–dependent signal within the lesion volume was extracted for each participant in the normative cohort and correlated with all brain voxels. Resulting individual r-maps were Fisher z-transformed, which were then used to generate a single connectivity t-map for each lesion. For step three, connectivity maps for each lesion were thresholded at a t-value of +/- 7 (corresponding to whole brain family-wise error [FWE]-corrected $p < 10^{-6}$), binarized (functionally connected or not, positive and negative connectivity separately as they may have different biological interpretation), and then overlapped to identify voxels connected to all 25 of our lesion locations causing CD (Figure 1). This three-step technique is summarized in Figure 2.

We also ran a number of lesion network mapping sub-analyses, excluding cases with ataxia or dysmetria (n=11), head tremor (n=6), hemiparesis (n=9), dystonia symptoms outside of cervical regions (n=6), and excluding cases not caused by ischemic stroke (n=15), to check that our findings were not being driven by these cases.

Specificity

To test for specificity to CD, we compared our results to two 'control' datasets of lesions not causing CD, as described previously (Joutsa et al., 2018a). First, we used a 'non-specific' dataset of lesions that were distributed throughout the brain without a common neuropsychiatric phenotype (n=135) (Corbetta et al., 2015). Second, we used a 'movement disorders' dataset, consisting of 73 lesions causing movement disorders other than dystonia: asterixis (n=30) (Kim, 2001; Laganiere et al., 2016); hemichorea-hemiballismus (n=29) (Laganiere et al., 2016), and freezing of gait (n=14) (Fasano et al., 2016).

We compared our network maps from lesions causing CD to these two control lesion datasets using two statistical methods: 1) a Liebermeister test, using voxel-based lesion-symptom mapping (VLSM) (Rorden et al., 2007); and 2) a two-sample t-test, using Statistical Parametric Mapping (SPM12; http://www.fil.ion.ucl.ac.uk/spm/software/spm12/) (Ashburner, 2012). Both statistical

approaches identify voxels that are significantly more or less connected to CD lesion locations than control lesion locations. The difference between these approaches is that the Liebermeister test analyzes voxels in a binary fashion (functionally connected or not), and is more commonly used in lesion analyses, while the t-test takes into account the strength of the connection, and is more commonly used in functional neuroimaging (Fasano et al., 2016). Because the Liebermeister test is used for binary image analyses, the group comparisons were conducted separately for positive and negative connectivity maps. Correction for multiple comparisons was conducted using whole brain voxel-level FWE for t-tests and false discovery rate (FDR) for Liebermeister tests across the whole brain voxels showing at least 10% overlap in the whole sample. Corrected p-values less than 0.05 were considered significant. Specificity analyses were restricted to voxels within the CD lesion network map (i.e. regions that were functionally connected to >90% [at least 23/25] of the lesions, as shown in Figure 3).

Regions of interest

To identify regions whose connectivity was both sensitive and specific to lesion locations causing CD, we performed a conjunction analysis of the above maps. These regions of interest (ROI) comprised of voxels that were connected to >90% of lesion locations causing CD, and also specific to CD across all four specificity analyses above (2 control groups x 2 statistical tests). Because the somatosensory cortex cluster that survived all four specificity tests was very small (14 voxels with the center of gravity at -8 -43 75 mm; Supplementary Figure 1D), voxels surviving 3 out 4 specificity analyses were used to define the somatosensory ROI.

The resultant cerebellar and somatosensory ROIs were then used in three analyses. First, we used a linear model to test whether connectivity between lesion locations and these ROIs were independent or redundant predictors of lesion induced CD. Note that our method of selecting these ROIs requires that connectivity to each ROI alone be a predictor of CD, but does not tell us whether these are independent predictors when combined in a linear model. Second, we used these ROIs to generate a network map that, by definition, encompasses lesion locations causing CD. To generate this map, we identified all voxels positively correlated with our cerebellar ROI, all voxels

negatively correlated with our somatosensory ROI, thresholded each map ($t > +/- 7$, voxelwise FWE corrected $p < 10^{-6}$), and identified voxels meeting both criteria. Lesion locations were overlaid on this map for illustration purposes. Finally, we used these ROIs to test whether these same regions, identified based on brain lesions, were abnormal in idiopathic CD (next section).

These ROIs were localized in greater anatomical detail using the Anatomy toolbox within SPM 12, utilizing cerebellar (Schmahmann et al., 1999; Diedrichsen, 2006; Diedrichsen et al., 2009), motor cortex (Geyer et al., 1996), and somatosensory cortex (Geyer et al., 2000; Grefkes et al., 2001) atlases. The cerebellar atlas utilizes nomenclature of Schmahmann et al. (1999), and also includes updates provided by Diedrichsen (2006) and Diedrichsen et al. (2009) to determine fissure and lobule locations.

Relevance to idiopathic cervical dystonia

Our cerebellar and somatosensory ROIs were used as seed regions to compare functional connectivity patterns between 39 idiopathic CD patients and 37 controls, in a dataset collated from two previously published rs-fcMRI studies of idiopathic CD (Delnooz et al., 2013; Prudente et al., 2016). The preprocessing of the rs-fcMRI data followed conventional methods and guidelines, including global signal regression (Fox et al., 2010; Murphy et al., 2016), but added an extra artifact-reduction step modified from prior PCA-based approaches (Behzadi et al., 2007) (Supplementary Methods).

Functional connectivity of patients and controls was compared using Permutation Analysis with Linear Models (PALM) with threshold-free cluster enhancement implemented in FSL software (Jenkinson et al., 2012). Permutation/randomization-based correction for multiple comparisons was selected to avoid inflated type I error rate associated with parametric cluster-level correction (Winkler et al., 2014; Eklund et al., 2016). Because patients often move more than controls, two metrics of in-scanner movement were included as subject-level covariates (relative frame-to-frame motion and cumulative frame-wise transposition) in addition to dataset (Fox et al., 2010). FWE corrected p-values less than 0.05 were considered significant. The z-

transformed values were extracted from all of the significant clusters to illustrate the direction of connectivity (positive or negative). Cumulative and relative in-scanner movement was compared using t-tests. P-values <0.05 were considered significant.

To assess specificity, we repeated this analysis using control ROIs derived from prior lesion network mapping studies of other neurological symptoms (Boes et al., 2015; Fasano et al., 2016; Fischer et al., 2016; Laganiere et al., 2016; Darby et al., 2017; Darby et al., 2018a; Darby et al., 2018b; Joutsa et al., 2018a). Control ROIs were derived in the same way as our dystonia ROIs, based on stronger connectivity to lesions causing a neurological symptom versus control lesions not causing the symptom. We identified 19 control ROIs from 8 prior papers, covering 11 different neurological symptoms (MNI coordinates of each control region are provided in the Supplementary Methods). Coordinates of one ROI were not reported in the original study (Laganiere et al., 2016), and were identified through visual comparison with an atlas brain. A 5mm radius sphere was generated at each coordinate, including center of gravity coordinates for our cerebellar and somatosensory ROIs. For each ROI, we repeated the above PALM analysis to identify differences in connectivity between patients with idiopathic CD and healthy controls. This resulted in a statistical map of T-values for each ROI. To quantify the overall magnitude of these connectivity abnormalities, we computed the average absolute T-value of all brain voxels. We compared the average absolute T-values of the 19 control ROIs to those from our two dystonia ROIs (cerebellar and sensorimotor) using two-sided one-sample T-tests with the null hypotheses that the control ROIs do not differ from either of the CD ROIs.

Relevance to deep brain stimulation treatment

Clusters of voxels near the globus pallidus significantly associated with clinical response to deep brain stimulation (DBS) for dystonia were extracted from a recent study (Reich et al., in press). Briefly, this study examined DBS electrode locations and stimulation sites from 105 patients with dystonia (53 CD, and 52 generalized or segmental dystonia patients). Patients were categorized as having a ‘good’ or ‘poor’ DBS response based on improvement in TWSTRS score (CD patients), or Burke-Fahn-Marsden Dystonia Rating Scale (generalized or segmental dystonia). Voxels significantly associated with good clinical response were identified for the full cohort

of dystonia patients ($p<0.01$), and also separately for subjects with CD ($p<0.05$). Although not emphasized in the paper by Reich et al., there was also a cluster of voxels significantly associated with poor DBS response in the full dystonia cohort ($p<0.01$). We tested whether 'good' clusters were functionally connected to our dystonia ROIs, and whether this connectivity was significantly greater than for the 'poor' cluster, using our resting state functional connectivity dataset from 1000 healthy young adults (Yeo et al., 2011; Holmes et al., 2015). Finally, we performed a voxelwise analysis to identify voxels significantly connected to the 'good' cluster, controlling for connectivity to the 'bad' cluster using partial correlation. Correlation to our cerebellar and sensorimotor ROIs, and to all brain voxels, was calculated as with lesions analyses, described in the previous paragraphs. The significance of the correlations was calculated using two-sided one-sample t-tests.

Results

Lesions causing cervical dystonia

We identified 25 cases of lesion-induced CD that met our inclusion/exclusion criteria (Table 1, Figure 1). Lesions occurred in a number of different brain locations including the cerebellum (11 lesions), brainstem (9), basal ganglia (8), thalamus (1), and occipital lobe (1). Some patients had lesions in multiple locations.

< Figure 1 here (drawn lesions) >

< Table 1 here (cases) >

Lesion network mapping

Each lesion location was converted into a lesion network map, and regions functionally connected to all or most lesion locations causing CD were identified (Figure 2). Despite heterogeneity in lesion locations, all lesions causing CD were part of a single functionally connected brain network. All 25 lesion locations were functionally connected (positively correlated) to the cerebellar vermis, dentate nucleus, cerebellar cortex, and midbrain (Table 2), and over 90% of lesion locations were functionally connected to the thalamus and globus pallidus (Figure 3A). All 25 lesion locations were also functionally connected, but negatively correlated, to the

right somatosensory cortex (Table 2), and over 90% of lesion locations were connected to the somatosensory cortex bilaterally, extending slightly into the motor cortex (Figure 3A). Medial and lateral clusters were found within the somatosensory cortex, consistent with previous reports of both a medial and lateral representation for the neck within the homunculus (Prudente et al., 2015; Prudente et al., 2016). Some smaller clusters of (positive and negative) functionally connected voxels were also present (Supplementary Figure 2). Results were unchanged when excluding cases with ataxia or dysmetria, head tremor, hemiparesis, dystonia symptoms outside of cervical regions, or cases not caused by ischemic stroke (Supplementary Figure 3).

< Figure 2 here (lesion network mapping technique) >

Connectivity to the cerebellum and somatosensory cortex was specific to lesion locations causing CD, compared to control lesion locations, independent of the statistical approach and control dataset (Figure 3B). We performed a conjunction analysis to identify regions whose connectivity was both sensitive and specific to lesion locations causing CD (see Methods - Regions of interest). This identified one ROI in the cerebellum, centered on the vermis of lobule IX (MNI coordinates 1 -54 -34 mm) and two ROIs in the somatosensory cortex / Brodmann's area 1 (MNI coordinates 45 -24 60 mm and -45 -28 59 mm) (Figure 3B). See Supplementary Table 2 for greater anatomical detail of these ROI locations, and Supplementary Figure 4 and 5 for overlay of our CD ROIs on cerebellar (Schmahmann et al., 1999; Diedrichsen, 2006; Diedrichsen et al., 2009), and sensorimotor cortex atlases (Geyer et al., 1996; Geyer et al., 2000; Grefkes et al., 2001). Our cerebellar ROI, connected to lesions causing CD, was in a different region of the cerebellum than a previously published ROI connected to lesions causing freezing of gait (Fasano et al., 2016) (Supplementary Figure 6).

< Figure 3 here (lesion network map) >

To test whether connectivity from the lesions to cerebellum and somatosensory cortex ROIs were independent or redundant predictors of lesion-induced CD, we included both as factors in a logistic regression model with a binary outcome variable (CD lesion vs. control lesion). Cerebellum ROI connectivity was a strong independent

predictor of CD ($p = 0.002$), while somatosensory cortex ROI connectivity fell just short of our statistical threshold for independence ($p = 0.051$).

By definition, connectivity with our cerebellar and somatosensory ROIs defines a network that encompasses lesion locations causing CD while avoiding control lesions. To illustrate this, we constructed a map of voxels both positively correlated with our cerebellar ROI and negatively correlated with our somatosensory ROI. As expected, our lesion locations causing CD fell within this topographic distribution (Figure 4), although one lesion fell just at the boundary of this network (#8).

< Figure 4 here (CD network) >

Relevance to idiopathic cervical dystonia

The aforementioned cerebellar and somatosensory ROIs, identified based on brain lesions, were used as seed regions to test whether these same regions were abnormal in patients with idiopathic CD. Our seed ROI in the cerebellum showed abnormal connectivity to regions in the lateral sensorimotor cortex and operculum (Figure 5A, Supplementary Table 1). Our seed ROI in the somatosensory cortex showed abnormal connectivity to regions in the basal ganglia, thalamus, anterior cingulate, occipital cortex, and sensorimotor cortex (Figure 5B, Supplementary Table 1). Each of these connectivity abnormalities involved a loss of normal negative or positive connectivity (Figure 5).

Our two ROIs derived from brain lesions causing CD showed greater abnormalities in idiopathic CD patients than 19 control ROIs derived from lesions causing other neurological symptoms (cerebellar ROI vs controls $p<0.001$; somatosensory ROI vs controls $p<0.001$). Average absolute T-values for all ROIs are presented in Supplementary Table 3.

There was no difference in cumulative ($p=0.69$) or relative ($p=0.22$) in-scanner movement between CD patients and healthy volunteers.

< Figure 5 here – relevance to idiopathic CD >

Relevance to DBS treatment

Finally, we examined whether our cerebellar and somatosensory ROIs, derived from focal brain lesions and abnormal in patients with idiopathic CD, were relevant to DBS treatment (Figure 6). Our cerebellar ROI was positively connected to DBS sites associated with good clinical response in CD patients ($p<0.001$) and in dystonia patients in general ($p<0.001$), and significantly more connected to DBS sites associated with good, compared to poor, clinical response ($p=0.03$). Our somatosensory ROI was negatively connected with the optimal DBS site for treating CD ($p<0.001$) and dystonia in general ($p<0.001$) and significantly more negatively connected to DBS sites associated with good, compared to poor, responses ($p<0.001$). Functional connectivity with these DBS sites matched the spatial topography of our CD network derived from focal brain lesions (Figure 6).

< Figure 6 here – relevance to DBS >

Discussion

There are several noteworthy findings. First, lesions causing CD are found in heterogeneous brain locations, but are part of a single functionally-connected brain network. Second, this network is defined by positive connectivity to the cerebellum and negative connectivity to somatosensory cortex, a pattern that is specific to lesions causing CD compared to control lesions. Finally, this network is abnormal in patients with *idiopathic* CD, and also matches the connectivity pattern of DBS sites associated with dystonia symptom improvement. These findings suggest a shared neuroanatomical network for CD independent of symptom etiology, and illustrate how lesion network mapping can guide the search for brain abnormalities and treatment targets in non-lesion patients with similar neurological symptoms.

Lesion network mapping in cervical dystonia

It is well known that lesions causing CD can occur in different brain locations (LeDoux et al., 2003), and connectivity with the lesion locations has been hypothesized to play a role in explaining this phenomenon (LeDoux et al., 2003; Prudente et al., 2014). Lesion network mapping allows for direct testing of this

hypothesis by integrating brain connectivity into lesion analysis (Boes et al., 2015; Fox, 2018). This technique allows one to localize lesion-induced symptoms to networks, rather than individual brain regions, and has proven useful in localization of other movement disorders (Fasano et al., 2016; Laganiere et al., 2016; Joutsa et al., 2018a). In the present study, we localize CD to a single brain network defined by connectivity to the cerebellum and somatosensory cortex.

The cerebellum in cervical dystonia

It has been suggested that CD may arise from dysfunction of the cerebellum given its role in integrating motor and proprioceptive inputs to coordinate movement (LeDoux et al., 2003; Jinnah et al., 2006). This hypothesis is supported by fMRI abnormalities in the cerebellum in CD patients (Prudente et al., 2016; Li et al., 2017), Purkinje cell loss on human autopsy (Prudente et al., 2013), and rodent studies causing dystonia via the manipulation of the cerebellum (Pizoli et al., 2002; Calderon et al., 2011). The present study adds to this prior work by showing that all lesion locations causing CD are connected to the cerebellum, including the cerebellar cortex, vermis, and dentate nucleus (see Figure 3, Supplementary Table 2, Supplementary Figure 4).

Several studies have found normal cerebellar function or connectivity in idiopathic CD patients, or abnormal cerebellar function only in CD patients with tremor (Delnooz et al., 2013; Sadnicka et al., 2014; Antelmi et al., 2016; Bologna et al., 2016; Avanzino et al., 2018). Here, we found that all lesions causing CD were connected to the cerebellum, including cases with no head tremor (Supplementary Figure 3D). We also found abnormal cerebellar connectivity in our idiopathic CD rs-fMRI dataset, comprised of patients with minimal or no head tremor (Figure 5) (Delnooz et al., 2013; Prudente et al., 2016). One possible explanation for these discordant findings is that CD involves a specific region within the cerebellum, and other cerebellar regions can appear normal, or abnormal only in patients with tremor. Another possibility is that our lesion-based approach and larger cohort size allowed for increased sensitivity for cerebellar abnormalities in CD.

The somatosensory cortex in cervical dystonia

Prior work also implicates the somatosensory cortex in the pathophysiology of CD by demonstrating hyperactivity during head rotation (Prudente et al., 2016), increased plasticity to sensorimotor stimuli (Kojovic et al., 2013; Koch et al., 2014), and disinhibition (Inoue et al., 2004). It has been hypothesized that dystonia may result from increased proprioceptive input to the somatosensory cortex, leading to 'motor overflow' and co-contraction of muscles (Hallett, 2011; Kaňovský et al., 2011). Our finding that lesion locations are *negatively* correlated to the somatosensory cortex may be consistent with this hypothesis. The interpretation of negative correlations seen with fcMRI remains a matter of debate (Murphy et al., 2016), however negative correlations may represent brain regions that are suppressed during activation of competing regions (Fox et al., 2005). Based on this model, a lesion causing CD could result in a loss of the normal suppressive input from the lesion location to the somatosensory cortex, and therefore hyperactivity in this region.

Similar results are seen in lesion-induced hallucinations. Specifically, lesions causing visual or auditory hallucinations are negatively correlated with visual and auditory cortices, respectively (Boes et al., 2015). Other similarities exist between CD and hallucinations, including hyperactivity in the relevant sensory cortical area (Prudente et al., 2016; Zmigrod et al., 2016), and symptom improvement with sensory input. For example, visual and auditory hallucinations can improve with visual and auditory input (Teunisse et al., 1996; Corlett et al., 2009), while CD can improve with sensory or proprioceptive input, the so-called 'geste antagoniste' or sensory trick (Naumann et al., 2000; Schramm et al., 2004). The notion that CD may be a form of sensory or proprioceptive hallucination is highly speculative, but a testable hypothesis motivated by the present findings.

The basal ganglia in cervical dystonia

Our findings emphasize the importance of the cerebellum and somatosensory cortex in defining the CD network, but do not discount a role for the basal ganglia or other brain regions (Neychev et al., 2011). For example, 24 of 25 CD lesion locations were connected to the globus pallidus (see Figure 3A), an effective deep brain stimulation (DBS) target for CD (Volkmann et al., 2014). However, unlike the cerebellum and somatosensory cortex, connectivity to the basal ganglia was not specific to lesions

causing CD. This is not surprising given the role of the basal ganglia in other lesion-induced symptoms, including other movement disorders included in our 'control lesions' sample (Fasano et al., 2015; Laganiere et al., 2016). Similarly, treatments targeting the basal ganglia such as DBS are not specific to CD, but are also effective for other movement disorders (Follett et al., 2010). As such, connectivity to the cerebellum and somatosensory cortex are the most sensitive and specific markers of lesion-induced CD, but this does not discount the involvement of the basal ganglia in CD.

A two-hit model of cervical dystonia

The involvement of two distinct brain regions differs from previous 'lesion network mapping' studies of movement disorders where lesion locations were characterized by connectivity to just a single location (Fasano et al., 2016; Laganiere et al., 2016; Joutsa et al., 2018a). Results in CD are similar to lesion network mapping of more complex symptoms such as hallucinations (Boes et al., 2015), delusions (Darby et al., 2017), and criminality (Darby et al., 2018a), in which lesion locations were positively connected to one brain region and negatively connected to another. Connectivity of lesion locations to two different regions is consistent with two-hit models of symptom generation. For example, delusions are thought to require both a disruption in sensory processing and belief evaluation (Coltheart, 2010). A two-hit model has previously been proposed for dystonia (Schicatano et al., 1997; Jinnah et al., 2006; Neychev et al., 2008), but these models usually implicate the cerebellum and basal-ganglia. Our results suggest that CD symptoms may be caused by combined dysfunction of the cerebellum and somatosensory cortex.

Relevance to idiopathic cervical dystonia

One of our most important findings is the demonstration that lesion network mapping can guide analyses of patients with similar symptoms but without brain lesions, to identify a common neuroanatomical substrate. Idiopathic and acquired CD can be indistinguishable clinically (LeDoux et al., 2003), however unlike acquired CD where symptoms are causally linked to a lesion location, the brain regions causing idiopathic CD are difficult to isolate. Neuroimaging studies have implicated many different regions and connections between regions (Delnooz et al., 2013; Prudente et al., 2016;

Li et al., 2017), and determining which abnormalities are causing symptoms, compensating for symptoms, or incidentally correlated with symptoms can prove difficult or impossible. By starting with brain lesions, we identified a network causally linked to CD, defined by connectivity to the cerebellum and somatosensory cortex. Connectivity with these two regions thus defines a distributed brain network that encompasses lesion locations causing CD. The fact that connectivity with these same two regions is abnormal in idiopathic CD suggests a shared neuroanatomical substrate for idiopathic and acquired CD. Note that connectivity need not be abnormal *between* these two regions to establish this convergence, as it is connectivity between each region and all other brain voxels that defines the CD network. Finally, the fact that these two regions were significantly more abnormal than 19 other control regions suggests that lesion network mapping can help identify the location of key abnormalities in patients with similar symptoms but who do not have brain lesions.

This shared neuroanatomical substrate generates testable hypotheses for identifying and refining therapeutic targets in CD. For example, DBS to the GPi is effective for many but not all patients with CD (Kiss et al., 2007; Volkmann et al., 2014). Here we show that GPi DBS electrode locations associated with good clinical response have positive connectivity to the cerebellum and negative connectivity to the somatosensory cortex. This importance of brain connectivity in mediating DBS response is reminiscent of recent work in Parkinson's Disease (Horn et al., 2017; Joutsa et al., 2018a). Similarly, transcranial magnetic stimulation to the lateral cerebellum has shown some promise in patients with CD (Koch et al., 2014), and this target could possibly be refined based on the current results. Finally, the present results highlight the somatosensory cortex as a potential therapeutic target easily amenable to noninvasive brain stimulation. Though this target has yet to be tried in CD to our knowledge, there is some evidence that this target may provide benefit to patients with hand dystonia (Havrankova et al., 2010).

Limitations

A number of limitations should be acknowledged. First, although we conducted a systematic search to collect a representative sample of brain lesions causing CD, we cannot exclude a publication bias, as lesions in locations previously linked to CD may

be more likely to be reported. Second, there are potential limitations regarding lesion network mapping, such as drawing lesions by hand, using 2D instead of real 3D lesions, and the use of a normative connectome dataset. However, these limitations have been addressed in detail previously and found to have little impact on lesion network mapping results (Boes et al., 2015; Darby et al., 2018a). Next, interpretations based on functional connectivity data are based on indirect evidence, which constrains the causal interpretation of lesion network mapping findings (Fox, 2018), and of functional connectivity abnormalities observed in patient populations (Fox et al., 2010; Delnooz et al., 2013; Prudente et al., 2016). Finally, there have been numerous brain regions implicated in idiopathic CD based on neuroimaging (Prudente et al., 2016; Li et al., 2017), and it is yet to be determined whether the subset of regions connected to causal brain lesions identified in this study will prove more central to symptom pathophysiology, or more useful as treatment targets.

Conclusions

Lesion locations causing CD are part of a common brain network defined by connectivity to the cerebellum and the somatosensory cortex. This network, identified based on brain lesions, is abnormal in patients with idiopathic CD, and aligns with effective DBS sites. We suggest a shared substrate for idiopathic and acquired CD, propose a two-hit model of CD symptoms, and provide testable hypotheses for improving treatment.

Acknowledgments

The authors wish to thank Prof. Jens Volkmann for sharing DBS localization data, and for valuable feedback on manuscript drafts.

Funding

The present work was supported by the Dorothy Feiss Dystonia Research Fund and the Dystonia Medical Research Foundation. DC was supported by a Victoria Fellowship awarded by the Veski Foundation. JJ was supported by the Academy of Finland (Grant #295580), the Finnish Medical Foundation, and the Orion Research Foundation. MDF was supported by K23 NS083741, R01 MH113929, the Nancy Lurie Marks Foundation, the National Parkinson's Foundation, and the Mathers

Foundation. CD receives support from Prinses Beatrix fund and Hersenstichting. BPCvdW receives research support from Hersenstichting, ZonMW, Bioblast Pharma, and Radboud University Medical Centre. HL is supported by the NIH grants 1R01NS091604, P50MH106435, Beijing Municipal Science & Technology Commission grant No. Z161100002616009; and National Natural Science Foundation of China grant No. 81790652. JJ reports travel grants from Abbvie and Orion. HJ has active or recent grant support from the US government (National Institutes of Health), private philanthropic organizations (the Benign Essential Blepharospasm Research Foundation, Cure Dystonia Now), academically-oriented institutions (the Dystonia Study Group), and industry (Cavion Therapeutics, Ipsen Pharmaceuticals, Retrophin Inc.). HJ has served on advisory boards or as a consultant for Abide Therapeutics, Allergan Inc., Psyadon Pharmaceuticals, Retrophin Inc., Saol Therapeutics, and Medtronic Inc. HJ has received honoraria or stipends for lectures or administrative work from the American Academy of Neurology, the Dystonia Medical Research Foundation, the International Neurotoxin Society, the International Parkinson's Disease and Movement Disorders Society, The Parkinson's Disease Foundation, and Tyler's Hope for a Cure. HJ serves on the Scientific Advisory Boards for Cure Dystonia Now, the Dystonia Medical Research Foundation, Lesch-Nyhan Action France, and Tyler's Hope for a Cure. He also is principle investigator for the Dystonia Coalition, which receives the majority of its support through NIH grant TR001456 from the Office of Rare Diseases Research at the National Center for Advancing Translational Sciences, and previously NS065701 from the National Institutes of Neurological Disorders and Stroke. The Dystonia Coalition has received additional material or administrative support from industry sponsors (Allergan Inc. and Merz Pharmaceuticals) as well as private foundations (The American Dystonia Society, Beat Dystonia, The Benign Essential Blepharospasm Foundation, Cure Dystonia Now, Dystonia Inc., Dystonia Ireland, The Dystonia Medical Research Foundation, The European Dystonia Federation, The Foundation for Dystonia Research, The National Spasmodic Dysphonia Association, and The National Spasmodic Torticollis Association). MMR was supported by the Interdisciplinary Center for Clinical Research (Z-3/64) of the University Hospital Würzburg and the German section of the International Federation of Clinical Neurophysiology. The authors report no competing interests.

References

Adolphs R. Human lesion studies in the 21st century. Neuron 2016; 90: 1151-1153.

Albanese A, et al. Phenomenology and classification of dystonia: a consensus update. Movement Disorders 2013; 28: 863-873.

Antelmi E, et al. Impaired eye blink classical conditioning distinguishes dystonic patients with and without tremor. Parkinsonism Relat Disord 2016; 31: 23-27.

Ashburner J. SPM: a history. Neuroimage 2012; 62: 791-800.

Avanzino L, et al. Adaptation of feedforward movement control is abnormal in patients with cervical dystonia and tremor. Clinical Neurophysiology 2018; 129: 319-326.

Batla A, et al. The role of cerebellum in patients with late onset cervical/segmental dystonia?-Evidence from the clinic. Parkinsonism Relat Disord 2015; 21: 1317-1322.

Behzadi Y, Restom K, Liau J, Liu TT. A component based noise correction method (CompCor) for BOLD and perfusion based fMRI. Neuroimage 2007; 37: 90-101.

Boes AD, et al. Network localization of neurological symptoms from focal brain lesions. Brain 2015; 138: 3061-3075.

Bologna M, et al. Effects of cerebellar theta-burst stimulation on arm and neck movement kinematics in patients with focal dystonia. Clin Neurophysiol 2016; 127: 3472-3479.

Calderon DP, Fremont R, Kraenzlin F, Khodakhah K. The neural substrates of rapid-onset Dystonia-Parkinsonism. Nature Neuroscience 2011; 14: 357-365.

Carrera E, Tononi G. Diaschisis: past, present, future. Brain 2014; 137: 2408-2422.

Coltheart M. The neuropsychology of delusions. Annals of the New York Academy of Sciences 2010; 1191: 16-26.

Corbetta M, et al. Common behavioral clusters and subcortical anatomy in stroke. Neuron 2015; 85: 927-941.

Corlett P, Frith CD, Fletcher P. From drugs to deprivation: a Bayesian framework for understanding models of psychosis. Psychopharmacology 2009; 206: 515-530.

Darby RR, Horn A, Cushman F, Fox MD. Lesion network localization of criminal behavior. Proceedings of the National Academy of Sciences 2018a; 115: 601-606.

Darby RR, Joutsa J, Burke MJ, Fox MD. Lesion network localization of free will. Proceedings of the National Academy of Sciences 2018b; 115: 10792-10797.

Darby RR, Laganiere S, Pascual-Leone A, Prasad S, Fox MD. Finding the imposter: brain connectivity of lesions causing delusional misidentifications. Brain: a journal of neurology 2017; 140: 497-507.
Delnooz CC, Pasman JW, Beckmann CF, van de Warrenburg BP. Task-free functional MRI in cervical dystonia reveals multi-network changes that partially normalize with botulinum toxin. PloS one 2013; 8: e62877.
Diedrichsen J. A spatially unbiased atlas template of the human cerebellum. Neuroimage 2006; 33: 127-138.
Diedrichsen J, Balsters JH, Flavell J, Cussans E, Ramnani N. A probabilistic MR atlas of the human cerebellum. Neuroimage 2009; 46: 39-46.
Eklund A, Nichols TE, Knutsson H. Cluster failure: why fMRI inferences for spatial extent have inflated false-positive rates. Proceedings of the National Academy of Sciences 2016; 113: 7900-7905.
Fasano A, Herman T, Tessitore A, Strafella AP, Bohnen NI. Neuroimaging of freezing of gait. Journal of Parkinson's disease 2015; 5: 241-254.
Fasano A, Laganiere SE, Lam S, Fox MD. Lesions causing freezing of gait localize to a cerebellar functional network. Annals of Neurology 2016; 81: 129-141.
Fischer DB, et al. A human brain network derived from coma-causing brainstem lesions. Neurology 2016; 10.1212/WNL. 0000000000003404.
Follett KA, et al. Pallidal versus subthalamic deep-brain stimulation for Parkinson's disease. New England Journal of Medicine 2010; 362: 2077-2091.
Fox MD. Mapping Symptoms to Brain Networks with the Human Connectome. New England Journal of Medicine 2018; 379: 2237-2245.
Fox MD, Greicius M. Clinical applications of resting state functional connectivity. Frontiers in systems neuroscience 2010; 4: 19.
Fox MD, et al. The human brain is intrinsically organized into dynamic, anticorrelated functional networks. Proceedings of the National Academy of Sciences of the United States of America 2005; 102: 9673-9678.
Galardi G, et al. Basal ganglia and thalamo□cortical hypermetabolism in patients with spasmodic torticollis. Acta neurologica Scandinavica 1996; 94: 172-176.
Geyer S, et al. Two different areas within the primary motor cortex of man. Nature 1996; 382: 805.

Geyer S, Schormann T, Mohlberg H, Zilles K. Areas 3a, 3b, and 1 of human primary somatosensory cortex: 2. Spatial normalization to standard anatomical space. Neuroimage 2000; 11: 684-696.
Grefkes C, Geyer S, Schormann T, Roland P, Zilles K. Human somatosensory area 2: observer-independent cytoarchitectonic mapping, interindividual variability, and population map. Neuroimage 2001; 14: 617-631.
Hallett M. Neurophysiology of dystonia: the role of inhibition. Neurobiology of disease 2011; 42: 177-184.
Havrankova P, et al. Repetitive TMS of the somatosensory cortex improves writer's cramp and enhances cortical activity. Neuroendocrinology Letters 2010; 31: 73-86.
Holmes AJ, et al. Brain Genomics Superstruct Project initial data release with structural, functional, and behavioral measures. Scientific data 2015; 2: 150031.
Holmes AL, et al. Superior colliculus mediates cervical dystonia evoked by inhibition of the substantia nigra pars reticulata. Journal of Neuroscience 2012; 32: 13326-13332.
Horn A, et al. Connectivity predicts deep brain stimulation outcome in Parkinson's disease. Annals of Neurology 2017; 82: 67-78.
Inoue K, et al. Disinhibition of the somatosensory cortex in cervical dystonia—decreased amplitudes of high-frequency oscillations. Clinical neurophysiology 2004; 115: 1624-1630.
Isaac K, Cohen JA. Post□traumatic torticollis. Neurology 1989; 39: 1642-1642.
Jenkinson M, Beckmann CF, Behrens TE, Woolrich MW, Smith SM. Fsl. Neuroimage 2012; 62: 782-790.
Jinnah H, Hess EJ. A new twist on the anatomy of dystonia The basal ganglia and the cerebellum? Neurology 2006; 67: 1740-1741.
Joutsa J, Horn A, Fox MD. Localizing Parkinsonism based on focal brain lesions. Brain 2018a;
Joutsa J, et al. Identifying therapeutic targets from spontaneous beneficial brain lesions. Annals of neurology 2018b;
Kajimoto Y, Miwa H, Ueno M, Kondo T. Sensorimotor hemiparesis with secondary cervical dystonia following lateral caudal medullary infarction without signs and symptoms of Wallenberg syndrome. J Neurol Sci 2004; 219: 167-168.

Kaňovský P, Rosales RL. Debunking the pathophysiological puzzle of dystonia–with special reference to botulinum toxin therapy. Parkinsonism & related disorders 2011; 17: S11-S14.
Kim JS. Asterixis after unilateral stroke: lesion location of 30 patients. Neurology 2001; 56: 533-536.
Kirton CA, Riopelle RJ. Meige syndrome secondary to basal ganglia injury: a potential cause of acute respiratory distress. The Canadian journal of neurological sciences. Le journal canadien des sciences neurologiques 2001; 28: 167-173.
Kiss ZH, et al. The Canadian multicentre study of deep brain stimulation for cervical dystonia. Brain 2007; 130: 2879-2886.
Koch G, et al. Effects of two weeks of cerebellar theta burst stimulation in cervical dystonia patients. Brain stimulation 2014; 7: 564-572.
Kojovic M, et al. Secondary and primary dystonia: pathophysiological differences. Brain 2013; 136: 2038-2049.
Laganiere S, Boes AD, Fox MD. Network localization of hemichorea-hemiballismus. Neurology 2016; 86: 2187-2195.
Lambrecq V, et al. Acute blepharospasm and torticollis associated with an ependymoma of the lateral ventricle. Movement Disorders 2010; 25: 653-655.
LeDoux M, Brady K. Secondary cervical dystonia associated with structural lesions of the central nervous system. Movement Disorders 2003; 18: 60-69.
Li Z, et al. Alterations of resting-state fMRI measurements in individuals with cervical dystonia. Human Brain Mapping 2017; 38: 4098–4108.
Loher TJ, Krauss JK. Dystonia associated with pontomesencephalic lesions. Mov Disord 2009; 24: 157-167.
Molho ES, Factor SA. Basal ganglia infarction as a possible cause of cervical dystonia. Movement disorders 1993; 8: 213-216.
Murphy K, Fox MD. Towards a consensus regarding global signal regression for resting state functional connectivity MRI. Neuroimage 2016; 154: 169-173.
Naumann M, Magyar□Lehmann S, Reiners K, Erbguth F, Leenders KL. Sensory tricks in cervical dystonia: perceptual dysbalance of parietal cortex modulates frontal motor programming. Annals of neurology 2000; 47: 322-328.
Naumann M, et al. Imaging the pre□and postsynaptic side of striatal dopaminergic synapses in idiopathic cervical dystonia: A SPECT STUDY Using [123I] epidepride and [123I] β□CIT. Movement Disorders 1998; 13: 319-323.

Neychev VK, Fan X, Mitev V, Hess EJ, Jinnah H. The basal ganglia and cerebellum interact in the expression of dystonic movement. Brain 2008; 131: 2499-2509.
Neychev VK, Gross RE, Lehéricy S, Hess EJ, Jinnah H. The functional neuroanatomy of dystonia. Neurobiology of disease 2011; 42: 185-201.
Pizoli CE, Jinnah H, Billingsley ML, Hess EJ. Abnormal cerebellar signaling induces dystonia in mice. Journal of Neuroscience 2002; 22: 7825-7833.
Plant G, Kermode A, Du Boulay E, McDonald W. Spasmodic torticollis due to a midbrain lesion in a case of multiple sclerosis. Movement disorders 1989; 4: 359-362.
Prudente C, Hess E, Jinnah H. Dystonia as a network disorder: what is the role of the cerebellum? Neuroscience 2014; 260: 23-35.
Prudente C, et al. Neuropathology of cervical dystonia. Experimental neurology 2013; 241: 95-104.
Prudente C, et al. Neural Substrates for Head Movements in Humans: A Functional Magnetic Resonance Imaging Study. The Journal of Neuroscience 2015; 35: 9163-9172.
Prudente C, et al. A Functional Magnetic Resonance Imaging Study of Head Movements in Cervical Dystonia. Front Neurol 2016; 7: 201.
Reich M, et al. Probabilistic mapping of the antidystonic effect of pallidal neurostimulation: a multicentre imaging study Brain in press;
Richardson SP. Enhanced dorsal premotor–motor inhibition in cervical dystonia. Clinical Neurophysiology 2015; 126: 1387-1391.
Rorden C, Karnath H-O, Bonilha L. Improving lesion-symptom mapping. Journal of cognitive neuroscience 2007; 19: 1081-1088.
Sadnicka A, et al. Normal motor adaptation in cervical dystonia: a fundamental cerebellar computation is intact. Cerebellum 2014; 13: 558-567.
Schicatano EJ, Basso MA, Evinger C. Animal model explains the origins of the cranial dystonia benign essential blepharospasm. Journal of neurophysiology 1997; 77: 2842-2846.
Schmahmann JD, et al. Three-dimensional MRI atlas of the human cerebellum in proportional stereotaxic space. Neuroimage 1999; 10: 233-260.
Schramm A, Reiners K, Naumann M. Complex mechanisms of sensory tricks in cervical dystonia. Movement disorders 2004; 19: 452-458.
Schulze-Bonhage A, Ferbert A. Cervical dystonia as an isolated sign of a basal ganglia tumour. Journal of Neurology, Neurosurgery & Psychiatry 1995; 58: 108-109.

Schwartz M, De Deyn P, Pickut B. Cervical dystonia as a probable consequence of focal cerebral lesion. Movement disorders 1995; 10: 797-798.
Scott BL, Jankovic J. Delayed-onset progressive movement disorders after static brain lesions. Neurology 1996; 46: 68-74.
Teunisse RJ, Zitman F, Cruysberg J, Hoefnagels W, Verbeek A. Visual hallucinations in psychologically normal people: Charles Bonnet's syndrome. The Lancet 1996; 347: 794-797.
Tranchant C, Maquet J, Eber AM, Franck P, Warte JM. Cerebellar cavernous cervical dystonia and cross cortical diaschisis. Rev. Neurol. (Paris) 1991; 147: 599-602.
Volkmann J, et al. Pallidal neurostimulation in patients with medication-refractory cervical dystonia: a randomised, sham-controlled trial. The Lancet Neurology 2014; 13: 875-884.
von Monakow C. Die Lokalisation im Grosshirn und der Abbau der Funktion durch kortikale Herde. JF Bergmann.
Winkler AM, Ridgway GR, Webster MA, Smith SM, Nichols TE. Permutation inference for the general linear model. Neuroimage 2014; 92: 381-397.
Xiao J, et al. Mutations in CIZ1 cause adult onset primary cervical dystonia. Annals of neurology 2012; 71: 458-469.
Yeo B, et al. The organization of the human cerebral cortex estimated by intrinsic functional connectivity. Journal of neurophysiology 2011; 106: 1125-1165.
Zmigrod L, Garrison JR, Carr J, Simons JS. The neural mechanisms of hallucinations: A quantitative meta-analysis of neuroimaging studies. Neuroscience & Biobehavioral Reviews 2016; 69: 113-123.

Figure legends

Figure 1. Lesion locations causing cervical dystonia. A systematic literature search identified 25 cases of CD with an identifiable lesion location that could be traced onto a standard brain atlas. Case numbers correspond to those in Table 1.

Figure 2. Lesion network mapping technique. In step one, lesions causing CD were traced onto a standard atlas. In step two, connectivity between each lesion location and the rest of the brain was computed using a normative dataset of resting-state functional connectivity scans from 1000 healthy individuals, and a standard seed-

based approach. In step three, functional connectivity maps were thresholded, binarized (functionally connected or not), and overlapped to identify voxels connected to the greatest number of lesion locations.

Figure 3. Lesion network mapping of cervical dystonia. Figure 3A shows regions positively correlated (orange/yellow) or negatively correlated (blue/green) to lesion locations causing CD (thresholded at 90% or 23/25 cases). From L-R: thalamus (z = 10); globus pallidus (z = -2); midbrain (z = -13); cerebellum (z = -32), and somatosensory cortex (projected onto the brain surface). Figure 3B shows regions that are both sensitive and specific to lesions causing CD, with significantly greater (positive or negative) functional connectivity to lesion locations causing CD compared to control lesion locations (conjunction across 4 separate specificity analyses).

Figure 4. Lesions causing cervical dystonia are part of a commonly connected brain network. The combination of positive connectivity to our cerebellum region of interest and negative connectivity to our somatosensory region of interest defines a network of regions (blue) that encompasses 24 of 25 lesion locations causing CD (red). Case 8 falls immediately adjacent to this network.

Figure 5. Relevance to idiopathic cervical dystonia. Connectivity with our lesion-derived cerebellar region of interest (A, red) and somatosensory region of interest (B, blue) is abnormal in patients with idiopathic CD. Patients with idiopathic CD had a loss of negative functional connectivity from our cerebellar ROI to the right sensorimotor cortex (z = 38) and left operculum (orange/yellow) (A). Patients with idiopathic CD also had loss of negative connectivity from our somatosensory ROI to regions in the thalamus/basal ganglia and anterior cingulate (z = 12) (orange/yellow), and loss of positive connectivity to the sensorimotor and occipital cortex (z = 27) (blue/green). All images were corrected with Threshold-Free Cluster Enhancement $p_{FWE}<0.05$. Corresponding average (SEM) Fischer z transformed correlation coefficients (Fz) are shown in bar charts to illustrate the magnitude and direction of the group difference. CD=idiopathic cervical dystonia patients; HV=healthy volunteers.

Figure 6. Relevance to deep brain stimulation. Lesions causing CD are negatively connected to the somatosensory cortex and positively to the cerebellum (A). Globus pallidus interna deep brain stimulation locations associated with good clinical response in CD (B) and all dystonia patients (C) also show negative functional connectivity to the somatosensory cortex and positive functional connectivity to the cerebellum. Voxels associated with good response also show similar connectivity profile when controlling for voxels associated with poor response (D).

Table 1. Case characteristics of lesions causing cervical dystonia.

Case no.	First author (year)	Age/ gender	Lesion type	Lesion localization	Head position	Time until dystonia onset	Sensory symptoms	Other neurological abnormalities
1	LeDoux (2003)	55/M	Hemorrhage	R pons	L rotation	12 hours after admission due to acute onset hemiparesis and dysarthria.	Left hemihypesthesia. Diffuse hyperreflexia and bilateral Babinski responses.	Bilateral abducens palsy, left hemiparesis
2	LeDoux (2003)	42/F	Arachnoid cyst	L cerebello-pontine angle	L rotation, R laterocollis	3 to 4 months after two brief episodes of ataxia and tinnitus		Ataxia, tinnitus, migraine.
3	LeDoux (2003)	67/F	Infarct	Bilateral pons and caudal midbrain	R laterocollis, anterocollis	Several days after falling down her stairs and fracturing sternum and ribs	Hyperreflexia, brisk reflexes bilaterally in both the arms and legs. Plantar reflexes were equivocal bilaterally.	Dysarthria, R conjugate horizontal gaze deficit, R hemiparesis, R arm hypertonicity and tremor, spastic and ataxic gait, postural instability
4	LeDoux (2003)	72/M	Infarct	Bilateral pons, L thalamus, L occipital lobe	L rotation, mild retrocollis	One day after presentation to ER for 2-day history of altered mental status.	R hemihypesthesia	R homonymous hemianopsia, anomia, perseveration
5	Isaac (1989)	28/M	Posttraumatic hemorrhage	R putamen	L rotation, R shoulder elevation	4-5 years after auto-pedestrian accident	L plantar reflex was extensor, R arm pain developed after accident	Roving conjugate eye movements
6	Plant (1989)	30/F	Multiple sclerosis plaques	R midbrain, R cerebellar hemisphere	L rotation	One year after presentation for sensory disturbances in feet	Exaggerated lower limb tendon reflexes. Superficial sensation mildly impaired in all four limbs. Delayed visual-evoked potentials. L hemiparaesthesia. L	Multiple sclerosis, gait ataxia, optic atrophy, spastic paraparesis

							hemisensory disturbance to pain and temperature.	
7	Tranchant (1991)	53/F	Cavernous angioma	R cerebellar hemisphere	L rotation, anterocollis, laterocollis	3 years after initial presentation for hypotonia		R hemihypotonia
8	Molho (1993)	68/F	Infarct	L putamen	R rotation, mild L laterocollis	Acute onset, one year before scan		Intermittent head tremor
9	Molho (1993)	41/F	Infarct	L putamen	R rotation, R laterocollis, mild anterocollis	Acute onset 3 years before scan		Anxiety, depression
10	Schulze-Bonhage (1995)	40/M	Mixed grade III glioma	R basal ganglia and frontoparietal white matter	R laterocollis	2 years before lesion was detected	Numbness in the right temporoparietal region and, hypaesthesia in first R branch of the trigeminal nerve	L hemiparesis
11	Schwartz (1995)	63/M	Infarct	R caudate, R putamen, and internal capsule	R rotation, L laterocollis	Started gradually weeks before scan	Hyperreflexia, tendon reflexes increased bilaterally, ankle clonus, palmomental reflex positive bilaterally.	Involuntary movements of the mouth, tongue and chin muscles
12	Kajimoto (2004)	84/F	Infarct	L lateral caudal medulla	R laterocollis	10 days after presentation for dysarthria and gait disturbance	Decreased pain, touch, and temperature sensation on L side of face, body, and extremities. Decreased deep sensation on L side of body and extremities. Pain on L neck	L hemiparesis

13	Loher (2009)	31/M	Hemorrhage	R midbrain and pons. Superior cerebellar peduncle	R laterocollis, L rotation	3 months after hemorrhage	L hemihypaesthesia, deep tendon reflexes more reactive L side than R	L hemidystonia, orofacial dystonia, L hemiplegia. Dysarthria. L hemiparesis, L resting and kinetic tremor, jerky head tremor, R arm bradykinesia.
14	Loher (2009)	42/M	Posttraumatic hemorrhage	Midbrain and pons	R laterocollis, L rotation	4 months after hemorrhage	Deep tendon reflexes could not be elicited, L hemihypaesthesia	L hemidystonia, oculomotor disturbances, dysarthria, flaccid tetraparesis, ataxia, dysmetria, R postural and kinetic tremor
15	Loher (2009)	56/M	Hemorrhage	L pons, L middle cerebellar peduncle	R laterocollis, L rotation	1 month after hemorrhage	Hypesthesia of L face. R hemihypesthesia	L hemidystonia, blepharospasm, L facial palsy, dysarthria, L hemiataxia. R hemiparesis. Resting, postural and kinetic tremor of all extremities and head
16	Chang (2002)	23/M	Posttraumatic hemorrhage	L GPi	L rotation	3 years after hemorrhage		Mild R hemiparesis, mild dysarthria
17	Zadro (2008)	48/F	Infarct	L cerebellum	R rotation, anterocollis	Second day after hospital admission for vertigo, vomiting.		Ataxia. Horizontal, bidirectional, nystagmus.
18	Usmani (2011)	37/M	Hemorrhage	Vermis/R cerebellum	L rotation	15 months after hemorrhage		R horizontal nystagmus, ataxic gait, dysarthria, R dysmetria and difficulty with finger nose test.

19	O'Rourke (2006)	35/F	Infarct	L and R cerebellum	R rotation	3 days after hospital admission for weakness of legs, vertigo, vomiting, and blindness.		Bilateral blepharospasm, homonymous paracentral scotoma, truncal ataxia
20	Batla (2015)	56/F	Tumor	L cerebellum	R rotation	Information unavailable	Information unavailable	Dysmetria on finger nose test, dystonic tremor
21	Batla (2015)	33/M	Cyst	R cerebellum	R rotation	Information unavailable	Information unavailable	
22	Batla (2015)	58/M	Infarct	L cerebellum	R rotation	Information unavailable	Information unavailable	Dystonic tremor
23	Batla (2015)	29/M	Cyst	L cerebellum	L rotation	Information unavailable	Information unavailable	Dysmetria on finger nose test, dystonic tremor
24	Kirton (2001)	60/F	Infarct	L and R GP	Asymmetric and variable with rotation, antero-, retro-, and laterocollis	Blepharospasm began approximately 2 years after infarction. Dystonia progressed over several years to include oromandibular and cervical dystonia		Meige syndrome, dysmetria and dysdiadokinesia. Slow and wide gait
25	Lambrecq (2010)	23/M	Tumor (ependymoma)	R lateral ventricle, R caudate nucleus, and adjacent white matter	Anterocollis	Acute onset, scan taken within days		Bilateral blepharospasm

Table 2. Brain regions functionally connected to 25/25 lesions.

Regions positively connected with lesions

Voxels	**x**	**y**	**z**	**Brain region**
111	-6	-52	-36	Medial cerebellum
38	-33	-55	-29	L cerebellar cortex
22	14	-54	-36	Medial cerebellum
9	8	-17	-14	Midbrain
9	1	-25	-12	Midbrain
7	35	-52	-30	R cerebellar cortex
3	0	-20	-13	Midbrain
2	31	-58	-28	R cerebellar cortex
1	26	-24	-4	R lateral geniculate nucleus

Regions negatively connected with lesions

Voxels	**x**	**y**	**z**	
32	45	-30	58	Somatosensory cortex

Supplementary methods

Systematic search syntax

Search conducted in Pubmed in January 2017 within 'all fields': (cervical dystonia OR torticollis) AND (lesion OR lesions OR stroke OR infarct* OR ischem* OR ischaem* OR hemorrhag* OR haemorrhag* OR tumor OR tumour)

Relevance to idiopathic cervical dystonia - preprocessing pipeline

Resting-state fMRI data were processed using a pipeline modified from the procedure that has been described in previous studies (Yeo et al., 2011; Wang et al., 2013; Wang et al., 2015) which includes the following steps: (i) slice timing correction (SPM2; Wellcome Department of Cognitive Neurology, London, UK); (ii) rigid body correction for head motion with the FSL package (Jenkinson et al., 2002; Smith et al., 2004); (iii) normalization for global mean signal intensity across runs; and (iv) bandpass temporal filtering (0.01–0.08 Hz), head-motion regression, whole-brain signal regression, ventricular and white-matter signal regression and spatial smoothing [6mm full-width-at-half-maximum (FWHM)]. For group-level analysis, the resulting voxelwise correlation coefficient maps from each seed ROI were z-transformed.

Importantly, we extended the standard preprocessing procedure described above to further reduce noise. Specifically, we identified dominant principle components of background noise derived from principle component analysis (PCA). First, each subject's brain mask was dilated by one voxel (2mm) to ensure the full coverage of brain tissues. Second, signal in the dilated brain was removed from the BOLD runs of each subject and the PCA was performed using the remaining background signal. The assumption is that the remaining signal has no neural activity but a good representation of the background noise in the field of view. Third, the top ten principle components that contributed most to the variance (explaining about 80% of it) were identified. Finally, these principle components were removed from the BOLD runs with regression. Of note, this extra processing step was developed and tested using functional connectivity data from Parkinson's disease patients (who move excessively in the scanner) and then applied to the current cervical dystonia dataset without modification. No processing steps were manipulated to improve or change findings in

the current paper.

Another principle component based approach, component based noise correction method (CompCor), has previously been described as a method for noise reduction (Behzadi et al., 2007) Chai et al. (2012). used this method as a potential alternative to global signal regression, which is a common preprocessing technique to remove physiological and other noise in resting-state fMRI signal. However, one major difference between CompCor, which extracted the signal from the ventricles and white matter for the principle component analysis, and our method is that we used the signal from outside the brain as described above. Our method is an additional step after global signal regression and, thus, may be able to reduce external noise to a higher extent than CompCor.

The potential advantage of applying PCA to resting-state fMRI data lies in the approach of using background noise data only (after extracting the brain mask) to improve overall data quality without the risk of accidentally removing BOLD-signal representing neural activity within the brain. However, the extent to which PCA can contribute to data quality improvement will largely depend on the MRI scanner used, the electromagnetic environment and other physiological sources of background noise.

Structural data were processed using the FreeSurfer (version 5.3.0) software package, as previously described (Yeo et al., 2011). The version and processing environment were held constant for analysis of the full data sample. Structural and functional images were aligned using boundary-based registration registration (Greve et al., 2009) within the FsFast software package (http://surfer.nmr.mgh.harvard.edu/fswiki/FsFast).

Relevance to idiopathic cervical dystonia – control ROI analysis

To investigate whether our ROIs were selectively abnormal in idiopathic CD patients, we also analyzed a number of ‘control’ ROIs, derived from prior lesion network mapping studies (Boes et al., 2015; Fasano et al., 2016; Fischer et al., 2016; Laganiere et al., 2016; Darby et al., 2017; Darby et al., 2018a; Darby et al., 2018b; Joutsa et al.,

2018). The site of each ROI, and their MNI xyz coordinates, are as follows - peduncular hallucinosis (Boes et al., 2015): site of peak positive and negative connectivity from specificity analysis. ROI 1 (site of peak positive connectivity) = L anterior cingulate cortex (xyz MNI coordinate -12 32 14); ROI 2 (site of peak negative connectivity) = L inferior lateral occipital cortex (xyz -48 -64 -14). Auditory hallucinosis (Boes et al., 2015): site of peak positive and negative connectivity from specificity analysis. ROI 1 = L fronto-insular cortex (xyz -30 16 -18); ROI 2 = L superior temporal gyrus (xyz -52 -44 12). Central post-stroke pain (Boes et al., 2015): site of peak positive and negative connectivity from specificity analysis. ROI 1 = L insula (xyz -40 -6 -6); ROI 2 = R middle temporal gyrus (xyz 56 -20 -18). Subcortical aphasia (Boes et al., 2015): site of peak positive and negative connectivity from specificity analysis. ROI 1 = L inferior frontal gyrus (xyz -58 4 2); ROI 2 = L precuneus/white matter (xyz -18 -46 30). Criminal behavior (Darby et al., 2018a): site of peak positive and negative connectivity from specificity analysis. ROI 1 = frontal pole / ventromedial prefrontal cortex (xyz 4 66 8); ROI 2 = lingual / occipital, intraparietal sulcus (xyz -12 -76 -16). Coma (Fischer et al., 2016): peak intensity of two sites functionally connected to 'coma-specific' region, from specificity analysis. ROI 1: Anterior insula (xyz -40 12 -16); ROI 2: Pregenual Anterior Cingulate Cortex (xyz 0 38 12). Hemichorea-hemiballismus (Laganiere et al., 2016): site within posterolateral putamen significantly more connected to hemichorea-hemiballismus lesions than randomized lesions (specificity analysis). Coordinates were not reported in the manuscript, and therefore the site shown in Figure 3B (Laganiere et al., 2016) was traced by hand using FSL software (version 5.0.9) (as per the method of tracing lesions in the current paper). Free will (Darby et al., 2018b): site of peak connectivity from specificity analysis comparing connectivity of lesions disrupting volition (akinetic mutism/abulia) versus lesions causing hemiparesis, and site of peak connectivity from specificity analysis comparing connectivity of lesions disrupting agency (alien limb syndrome) versus lesions causing hemichorea. ROI 1 (volition ROI) = anterior cingulate cortex (xyz 2 18 32); ROI 2 (agency ROI) = precuneus (xyz 10 -40 50). Freezing of gait (FOG) (Fasano et al., 2016): brain region sensitive and specific to lesions causing FOG (Figure 2D&G, Fasano et al., 2016). ROI = dorsal medial cerebellum (xyz 16 -44 -26). Parkinsonism (Joutsa et al., 2018): brain region sensitive and specific to lesions causing parkinsonism. ROI = bilateral claustrum (xyz right claustrum 27 12 -12; xyz left claustrum -28 10 -13). Delusional

misidentifications (Darby et al., 2017): Site of peak positive and negative connectivity to lesions causing delusional misidentifications, and specific to lesions causing delusional misidentifications compared to lesions causing other neurological symptoms. ROI 1 = right frontal cortex (xyz 54 14 -10); ROI 2 = left retrosplenial cortex (xyz -6 -56 12).

References

Behzadi Y, Restom K, Liau J, Liu TT. A component based noise correction method (CompCor) for BOLD and perfusion based fMRI. Neuroimage 2007; 37: 90-101.

Boes AD, et al. Network localization of neurological symptoms from focal brain lesions. Brain 2015; 138: 3061-3075.

Chai XJ, Castañón AN, Öngür D, Whitfield-Gabrieli S. Anticorrelations in resting state networks without global signal regression. Neuroimage 2012; 59: 1420-1428.

Darby RR, Horn A, Cushman F, Fox MD. Lesion network localization of criminal behavior. Proceedings of the National Academy of Sciences 2018a; 115: 601-606.

Darby RR, Joutsa J, Burke MJ, Fox MD. Lesion network localization of free will. Proceedings of the National Academy of Sciences 2018b; 115: 10792-10797.

Darby RR, Laganiere S, Pascual-Leone A, Prasad S, Fox MD. Finding the imposter: brain connectivity of lesions causing delusional misidentifications. Brain: a journal of neurology 2017; 140: 497-507.

Fasano A, Laganiere SE, Lam S, Fox MD. Lesions causing freezing of gait localize to a cerebellar functional network. Annals of Neurology 2016; 81: 129-141.

Fischer DB, et al. A human brain network derived from coma-causing brainstem lesions. Neurology 2016; 10.1212/WNL. 0000000000003404.

Greve DN, Fischl B. Accurate and robust brain image alignment using boundary-based registration. Neuroimage 2009; 48: 63-72.

Jenkinson M, Bannister P, Brady M, Smith S. Improved optimization for the robust and accurate linear registration and motion correction of brain images. Neuroimage 2002; 17: 825-841.

Joutsa J, Horn A, Fox MD. Localizing Parkinsonism based on focal brain lesions. Brain 2018;

Laganiere S, Boes AD, Fox MD. Network localization of hemichorea-hemiballismus. Neurology 2016; 86: 2187-2195.

Smith SM, et al. Advances in functional and structural MR image analysis and implementation as FSL. Neuroimage 2004; 23: S208-S219.

Wang D, et al. Parcellating cortical functional networks in individuals. Nature neuroscience 2015; 18: 1853.

Wang D, Buckner RL, Liu H. Cerebellar asymmetry and its relation to cerebral asymmetry estimated by intrinsic functional connectivity. Journal of neurophysiology 2013; 109: 46-57.

Yeo B, et al. The organization of the human cerebral cortex estimated by intrinsic functional connectivity. Journal of neurophysiology 2011; 106: 1125-1165.

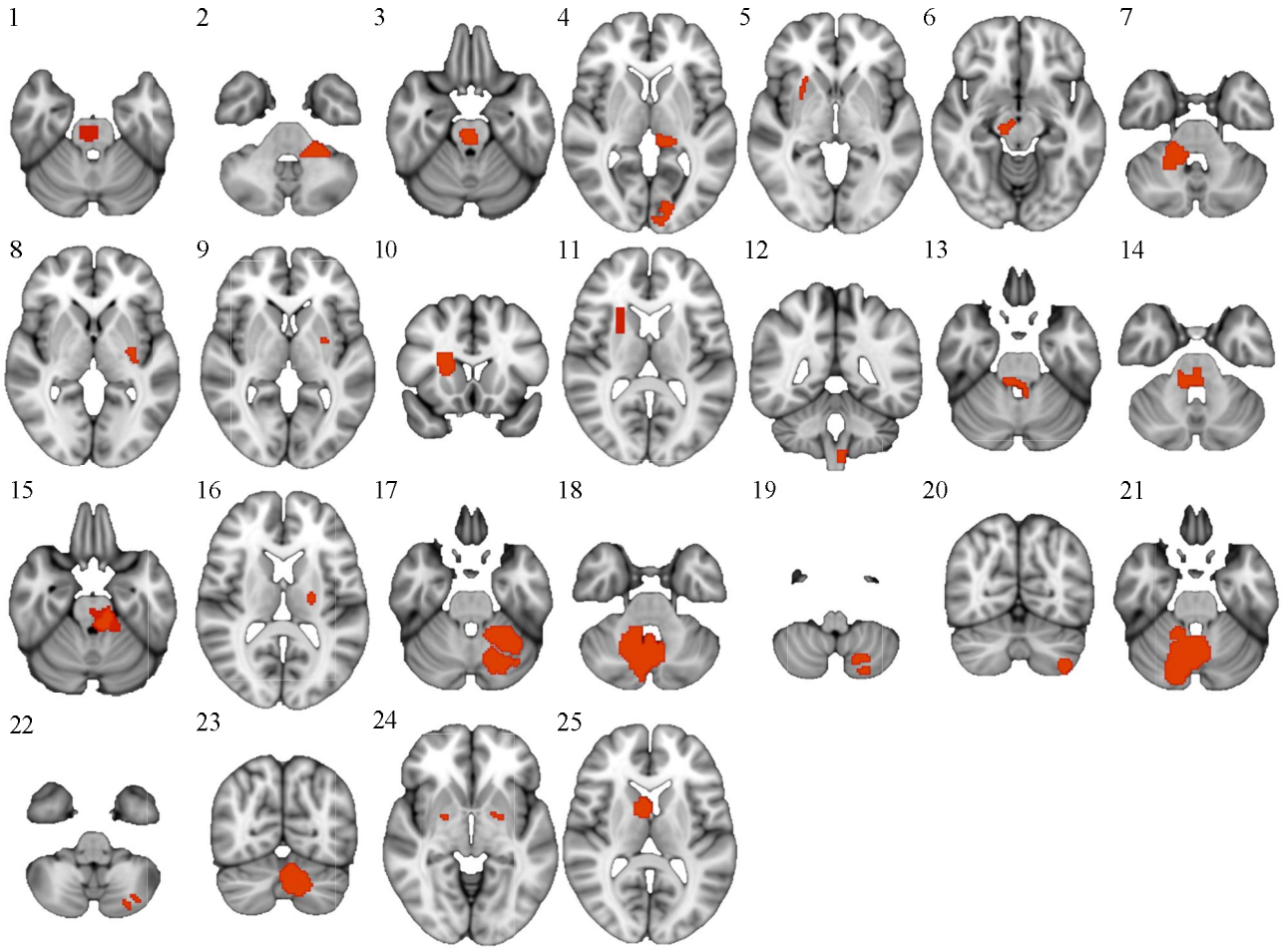
1
2
3
4
5
6
7
8
9
10
11
12
13
14
15
16
17
18
19
20
21
22
23
24
25

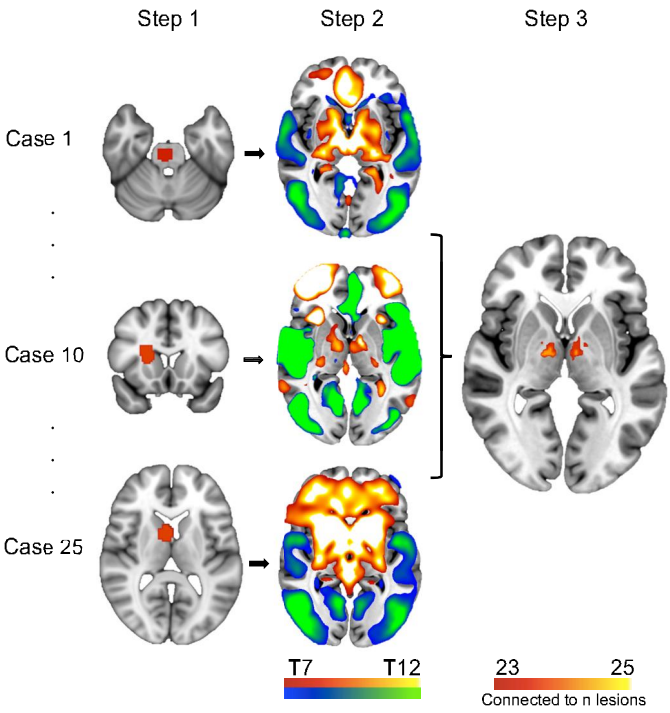
Step 1
Step 2
Step 3
Case 1
Case 10
Case 25
T7
T12
23
25
Connected to n lesions

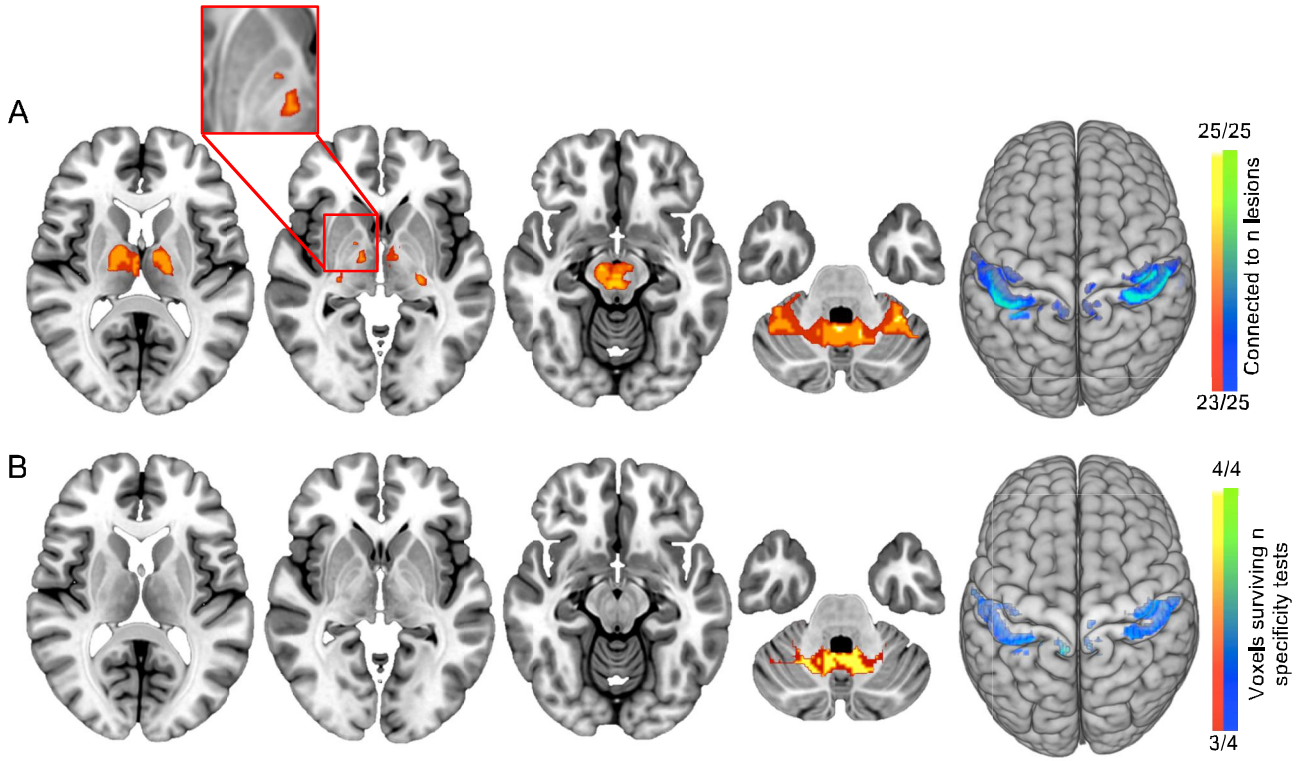
A
B
25/25
Connected to n lesions
23/25
4/4
Voxels surviving n specificity tests
3/4

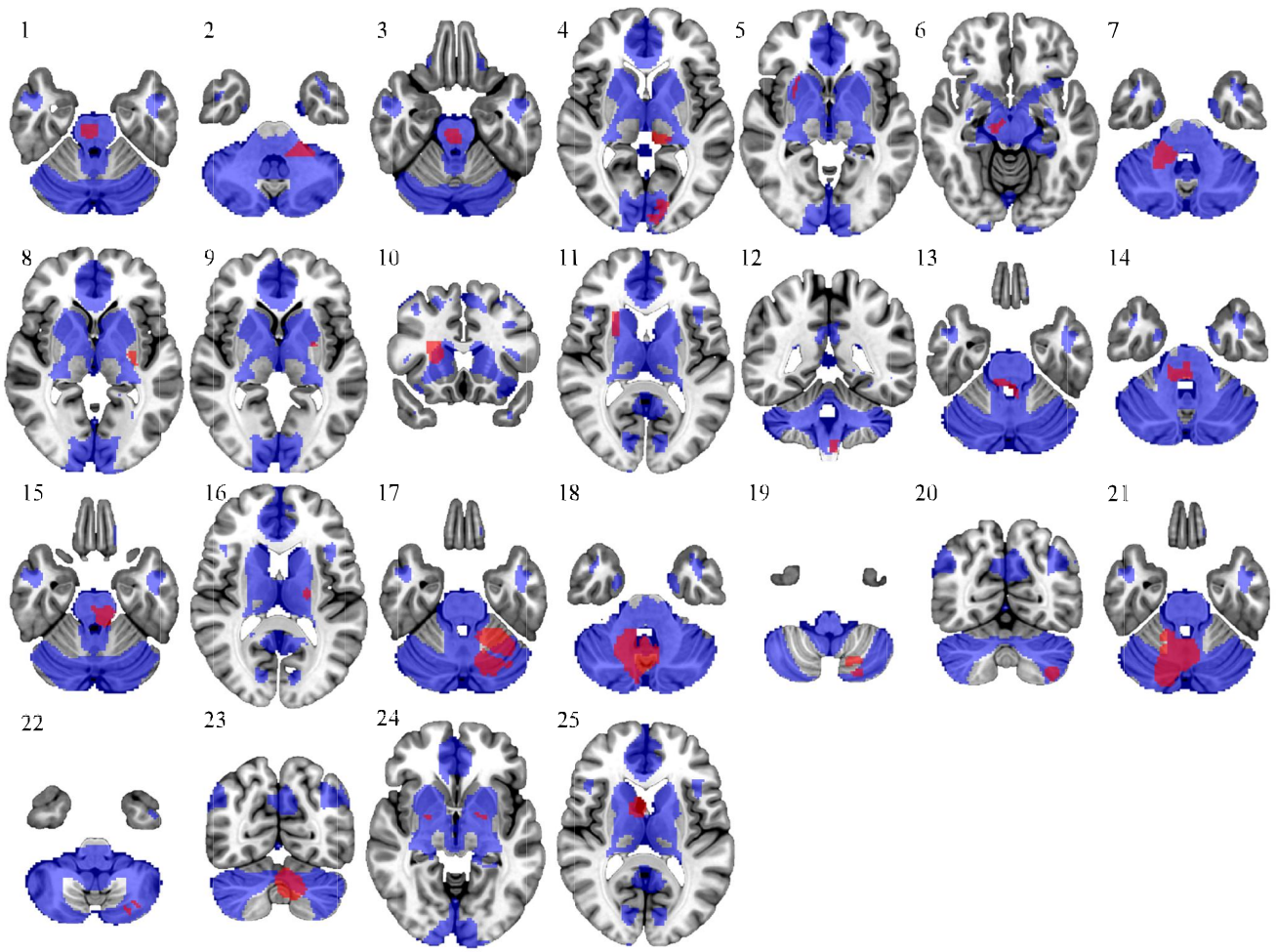
1
2
3
4
5
6
7
8
9
10
11
12
13
14
15
16
17
18
19
20
21
22
23
24
25

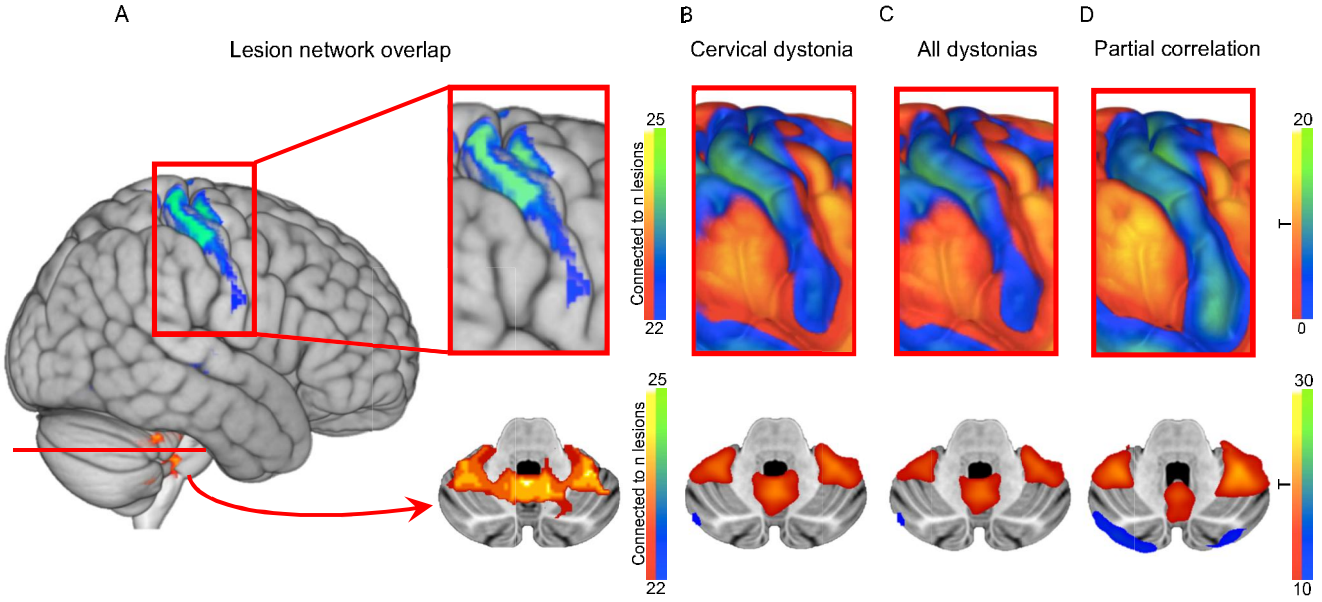
A
Lesion network overlap
B
Cervical dystonia
C
All dystonias
D
Partial correlation
25
Connected to n lesions
22
20
T
0
25
Connected to n lesions
22
30
T
10

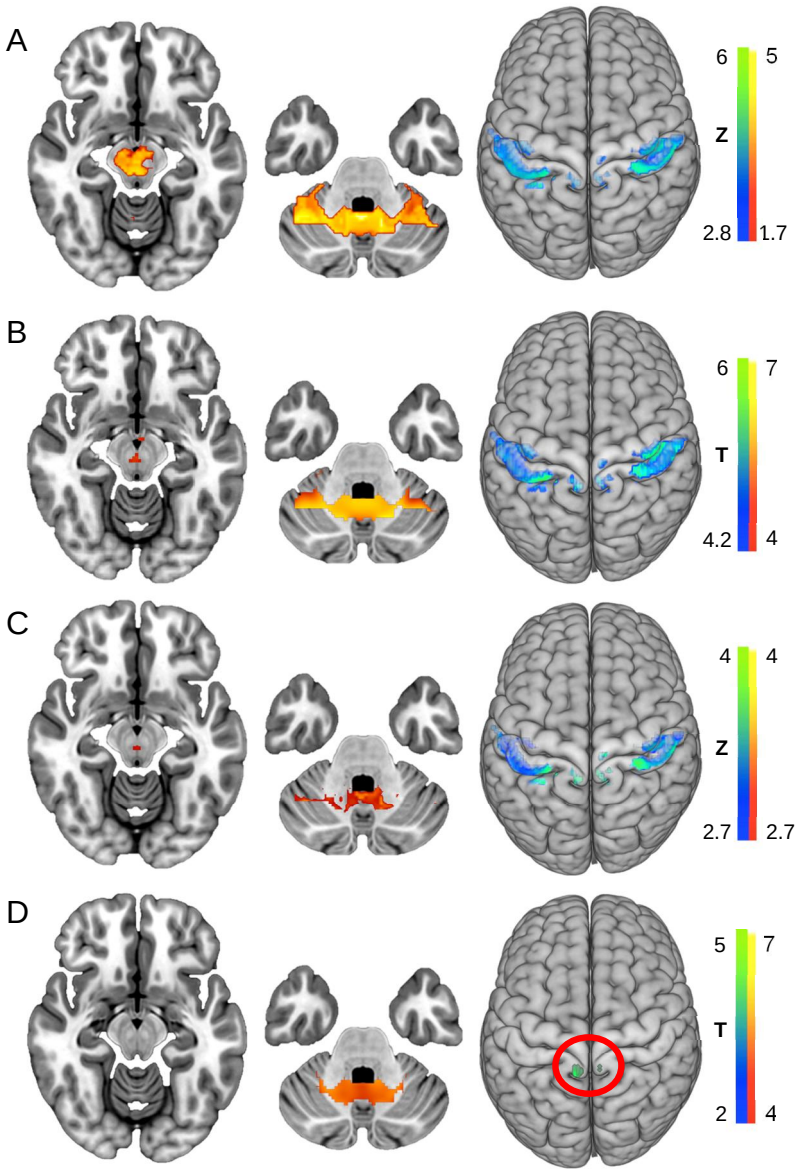

Supplementary Figure 1. Four tests identifying regions 'specific' to cervical dystonia. Figures 1A & 1B (tests 1&2) show regions with significantly greater (positive – orange/red, or negative – blue/green) functional connectivity from lesions causing cervical dystonia in comparison to non-specific lesions. 1A shows results using the Liebermeister test and 1B shows results using the t-test. 1C & 1D (tests 3&4) show the results of the same analyses, yet compared to other movement disorders. 1C shows results using the Liebermeister test and 4D shows results using the t-test. In each test, z = -13 for midbrain, and z = -32 for cerebellum. Somatosensory regions clusters are shown in surface space.

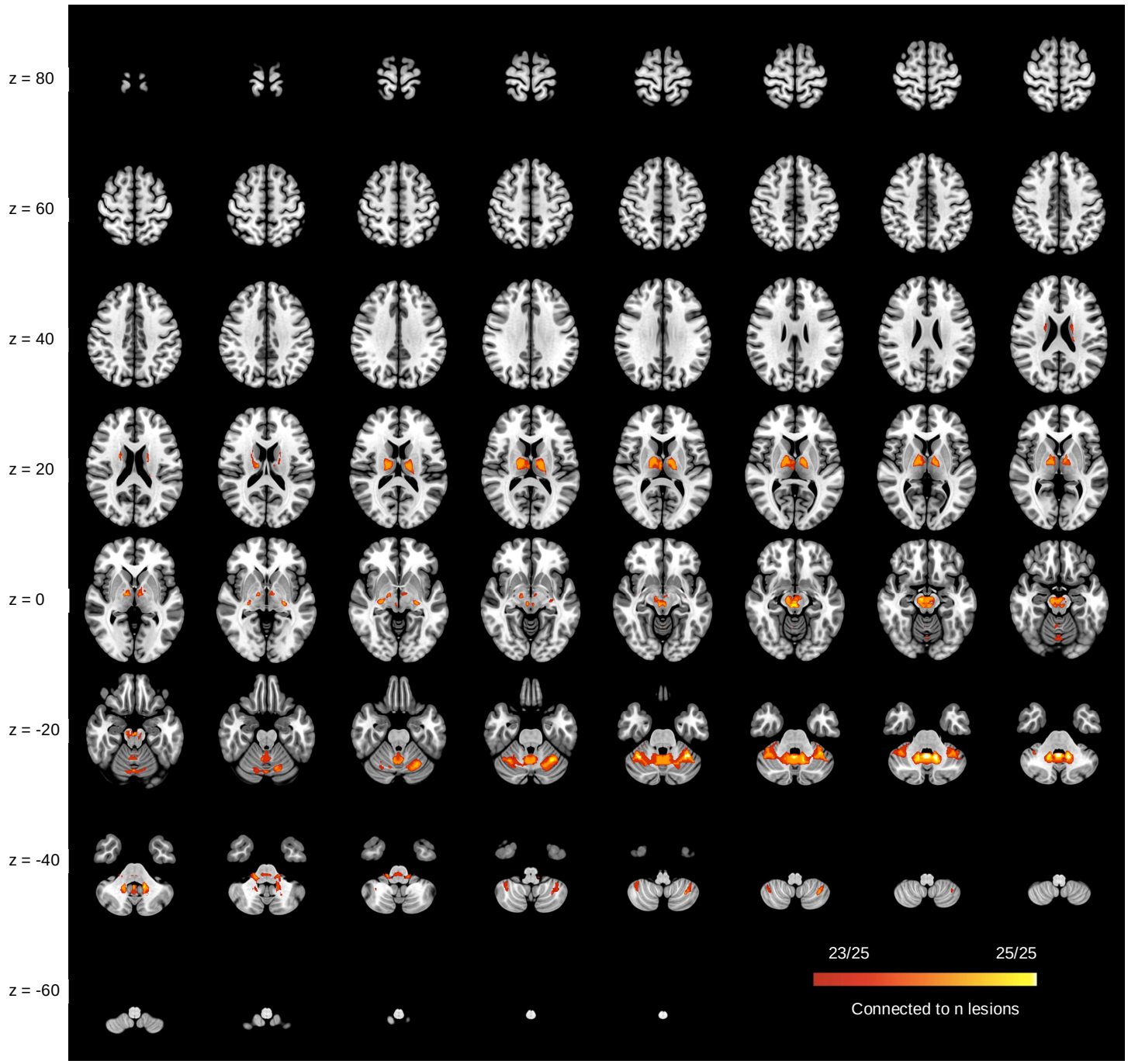

Supplementary Figure 2A. Lesion network map – positive correlations. Axial slices showing brain regions positively correlated to lesion locations in >90% (>23/25) of cases.

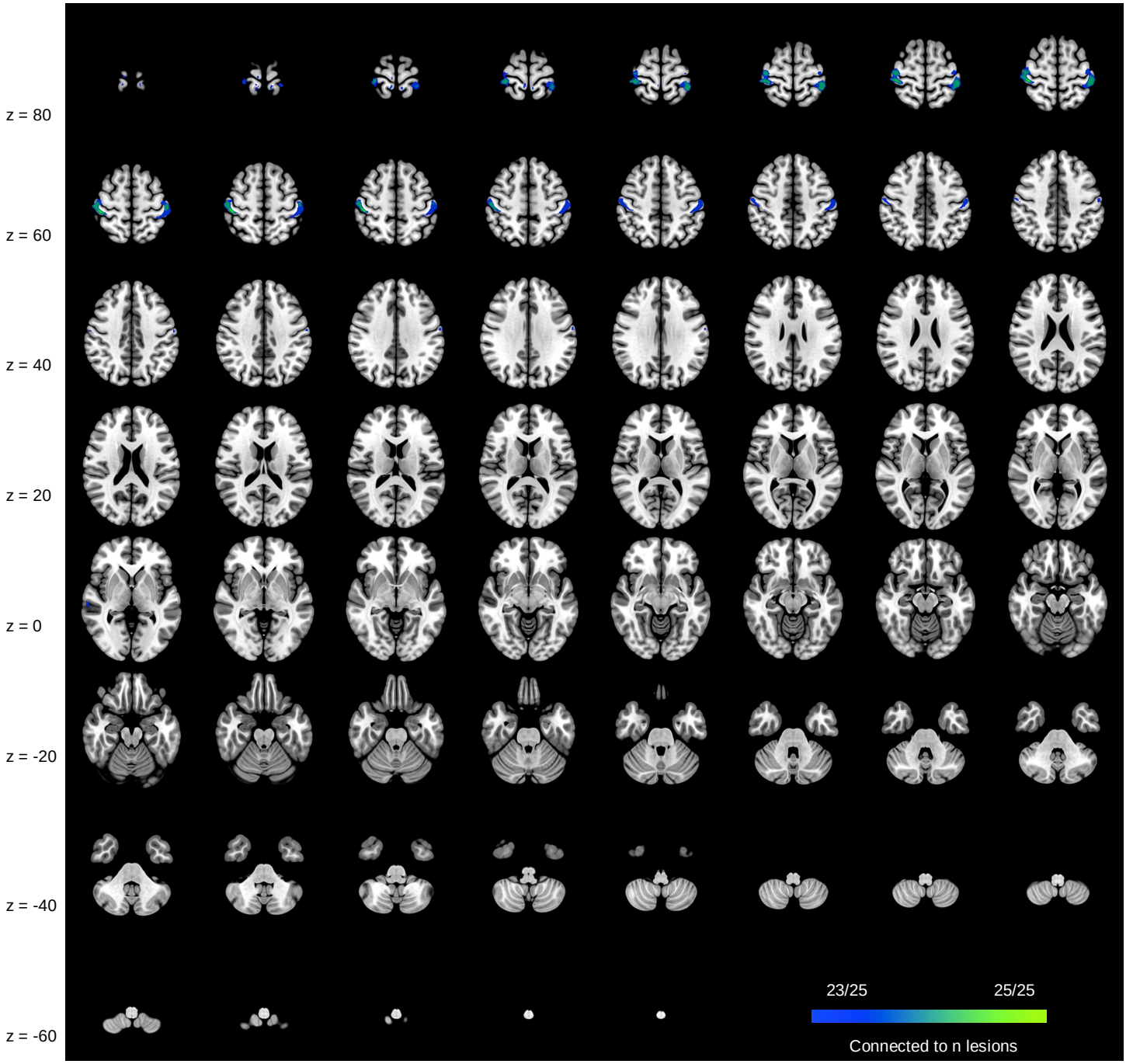

Supplementary Figure 2B. Lesion network map – negative correlations. Axial slices showing brain regions negatively correlated to lesion locations in >90% (>23/25) of cases.

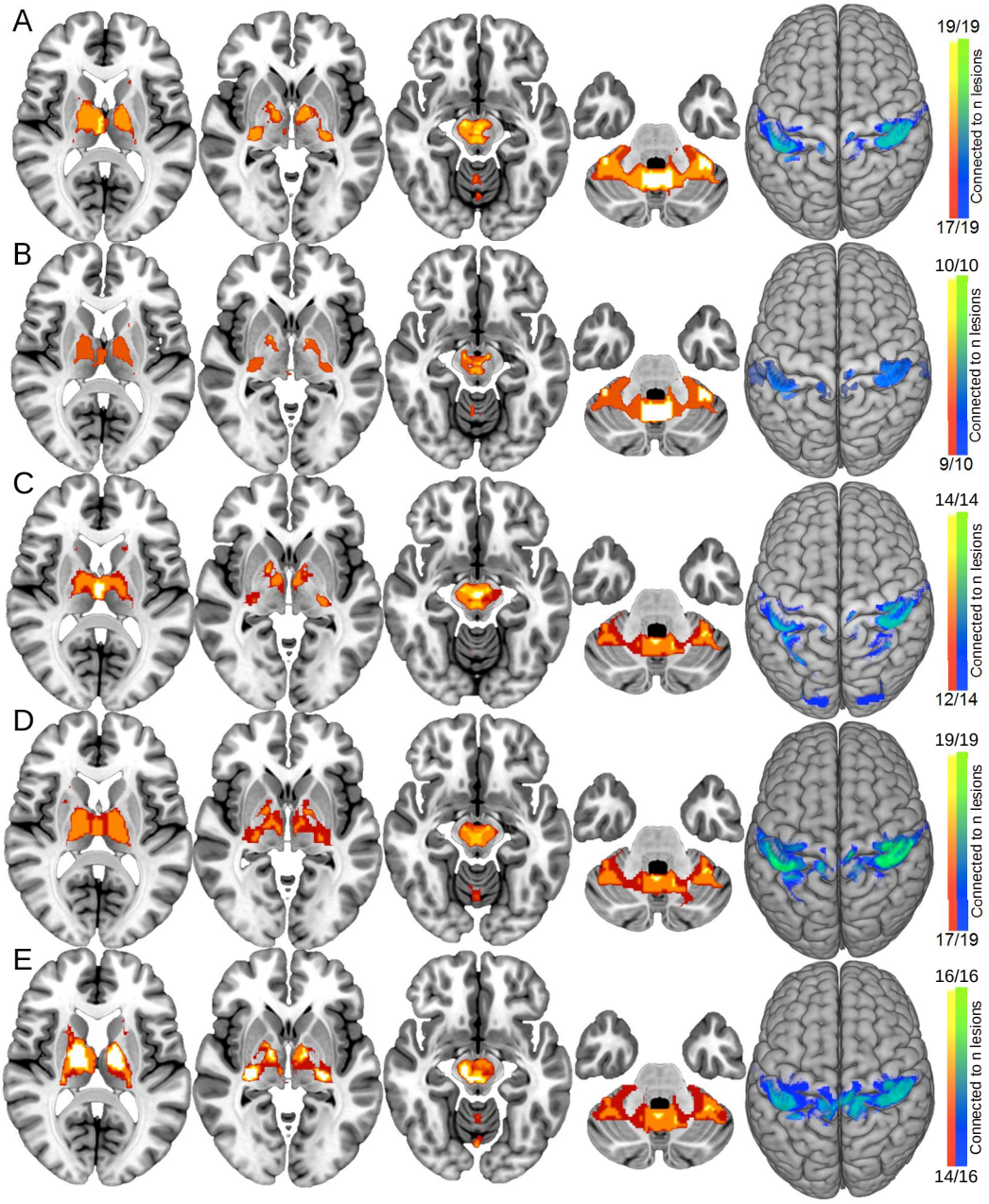

Supplementary Figure 3. Lesion network overlap validation in patient sub-groups. Figure A shows the lesion network map including only patients with *cervical* dystonia (excluding cases with dystonia to other body regions). Figure B shows the lesion network map in patients where cervical dystonia was caused only by ischemic stroke (excluding hemorrhages, tumors, cysts, plaques). Figure C shows map with cases of cervical dystonia including ataxia or dysmetria removed. Figure D shows map with cases of cervical dystonia with head tremor removed. Figure E shows cases of cervical dystonia with hemiparesis removed. These maps are almost identical to that in Figure 3, demonstrating that our results were not driven by these cases. Voxels positively correlated to lesions are shown in orange/red, and voxels and negatively correlated are shown in blue/green. From L-R: thalamus (z = 10); globus pallidus (z = -2) midbrain (z = -13); and cerebellum (z = -32), and somatosensory cortex (projected onto surface space).

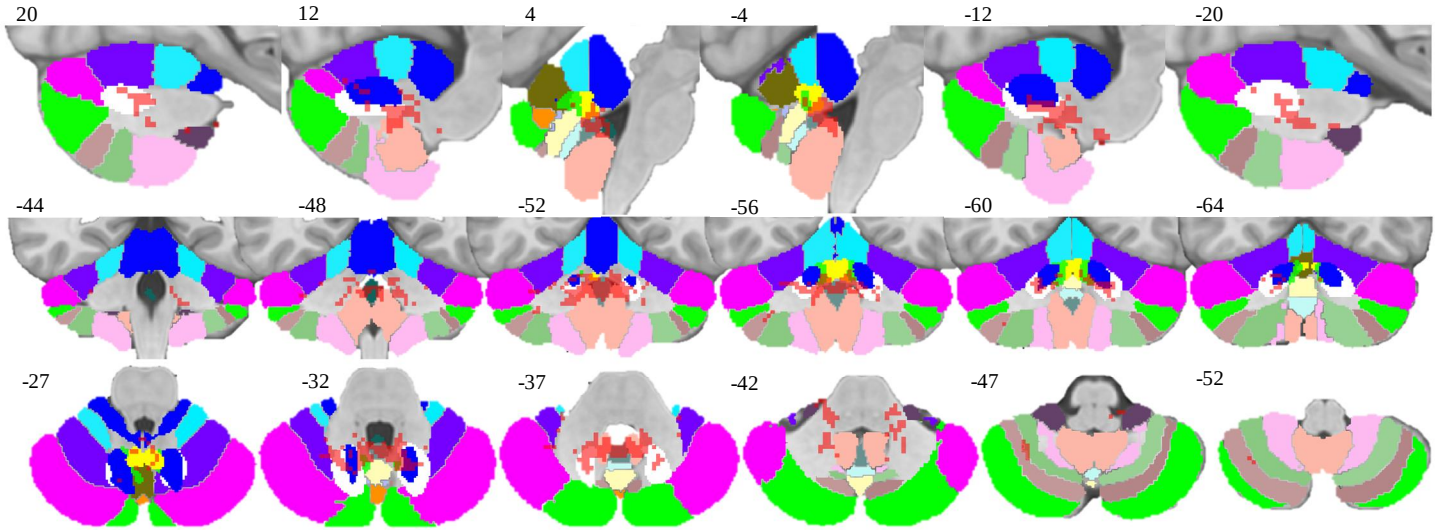

Supplementary Figure 4. Our 'specific' cervical dystonia cluster (Figure 3B) shown in red, overlaid onto cerebellar atlas (Schmahmann et al., 1999; Diedrichsen, 2006; Diedrichsen et al., 2009). Legend: Lobule IX (hemisphere); Dorsal Dentate Nucleus; Lobule IX (vermis); Lobule X (vermis); Lobule X (hemisphere); Interposed Nucleus; Ventral Dentate Nucleus; Fastigii Nucleus; Lobule VIIIb (hemisphere); Lobule VI (hemisphere); Lobule VIIIa (vermis). Legend shows regions that cerebellar cluster intersected, and is listed in order of highest to lowest intersection (by number of cerebellar voxels within each section).

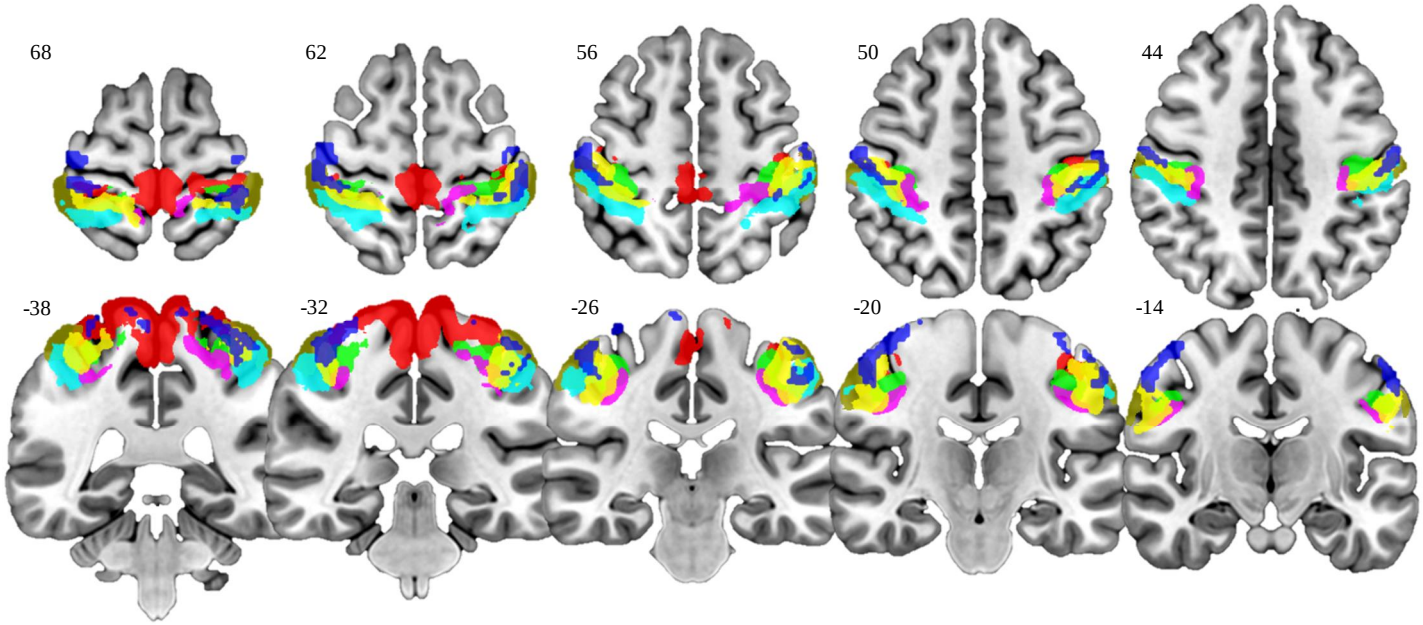

Supplementary Figure 5. Our 'specific' somatosensory ROI (blue) overlaid onto motor cortex (Geyer et al., 1996), and somatosensory cortex (Geyer et al., 2000; Grefkes et al., 2001) atlases. Red = Brodmann area (BA) 4a; green = BA 4p; mud brown = BA 1; aqua = BA 2; lavender = BA 3a; yellow = BA 3b. A quantitative breakdown of cluster locations within each BA is supplied in Supplementary Table 2.

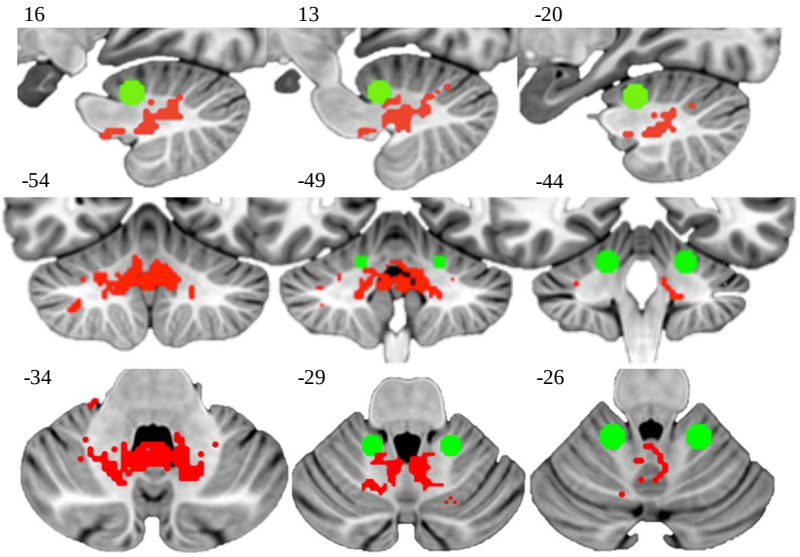

Supplementary Figure 6. cervical dystonia (CD) vs. freezing of gait (FOG) cerebellar ROIs. Figure shows ROI that was sensitive and specific to lesions causing CD (red) in comparison to the location of ROIs that were sensitive and specific to lesions causing FOG from Fasano et al., (2016). A 5mm sphere was created at these small FOG clusters located at xyz MNI coordinate 16 -44 -26 and -20 -44 -26 mm (see Figure 2D & 2G Fasano et al., 2016). Center of gravity in the largest CD cluster of 499 voxels was located at xyz MNI-coordinate 1 -54 -34 mm (see Figure 3B).

Supplementary table 1. Case characteristics of lesions causing cervical dystonia.

Case no.	First author (year)	Age/ gender	Lesion type	Lesion localization	Head position	Time until dystonia onset	Sensory symptoms	Other neurological abnormalities
1	LeDoux (2003)	55/M	Hemorrhage	R pons	L rotation	12 hours after admission due to acute onset hemiparesis and dysarthria.	Left hemihypesthesia. Diffuse hyperreflexia and bilateral Babinski responses.	Bilateral abducens palsy, left hemiparesis
2	LeDoux (2003)	42/F	Arachnoid cyst	L cerebello-pontine angle	L rotation, R laterocollis	3 to 4 months after two brief episodes of ataxia and tinnitus		Ataxia, tinnitus, migraine.
3	LeDoux (2003)	67/F	Infarct	Bilateral pons and caudal midbrain	R laterocollis, anterocollis	Several days after falling down her stairs and fracturing sternum and ribs	Hyperreflexia, brisk reflexes bilaterally in both the arms and legs. Plantar reflexes were equivocal bilaterally.	Dysarthria, R conjugate horizontal gaze deficit, R hemiparesis, R arm hypertonicity and tremor, spastic and ataxic gait, postural instability
4	LeDoux (2003)	72/M	Infarct	Bilateral pons, L thalamus, L occipital lobe	L rotation, mild retrocollis	One day after presentation to ER for 2-day history of altered mental status.	R hemihypesthesia	R homonymous hemianopsia, anomia, perseveration
5	Isaac (1989)	28/M	Posttraumatic hemorrhage	R putamen	L rotation, R shoulder elevation	4-5 years after auto-pedestrian accident	L plantar reflex was extensor, R arm pain developed after accident	Roving conjugate eye movements
6	Plant (1989)	30/F	Multiple sclerosis plaques	R midbrain, R cerebellar hemisphere	L rotation	One year after presentation for sensory disturbances in feet	Exaggerated lower limb tendon reflexes. Superficial sensation mildly impaired in all four limbs. Delayed visual-evoked potentials. L hemiparaesthesia. L	Multiple sclerosis, gait ataxia, optic atrophy, spastic paraparesis

							hemisensory disturbance to pain and temperature.	
7	Tranchant (1991)	53/F	Cavernous angioma	R cerebellar hemisphere	L rotation, anterocollis, laterocollis	3 years after initial presentation for hypotonia		R hemihypotonia
8	Molho (1993)	68/F	Infarct	L putamen	R rotation, mild L laterocollis	Acute onset, one year before scan		Intermittent head tremor
9	Molho (1993)	41/F	Infarct	L putamen	R rotation, R laterocollis, mild anterocollis	Acute onset 3 years before scan		Anxiety, depression
10	Schulze-Bonhage (1995)	40/M	Mixed grade III glioma	R basal ganglia and frontoparietal white matter	R laterocollis	2 years before lesion was detected	Numbness in the right temporoparietal region and, hypaesthesia in first R branch of the trigeminal nerve	L hemiparesis
11	Schwartz (1995)	63/M	Infarct	R caudate, R putamen, and internal capsule	R rotation, L laterocollis	Started gradually weeks before scan	Hyperreflexia, tendon reflexes increased bilaterally, ankle clonus, palmomental reflex positive bilaterally.	Involuntary movements of the mouth, tongue and chin muscles
12	Kajimoto (2004)	84/F	Infarct	L lateral caudal medulla	R laterocollis	10 days after presentation for dysarthria and gait disturbance	Decreased pain, touch, and temperature sensation on L side of face, body, and extremities. Decreased deep sensation on L side of body and extremities. Pain on L neck	L hemiparesis

13	Loher (2009)	31/M	Hemorrhage	R midbrain and pons. Superior cerebellar peduncle	R laterocollis, L rotation	3 months after hemorrhage	L hemihypaesthesia, deep tendon reflexes more reactive L side than R	L hemidystonia, orofacial dystonia, L hemiplegia. Dysarthria. L hemiparesis, L resting and kinetic tremor, jerky head tremor, R arm bradykinesia.
14	Loher (2009)	42/M	Posttraumatic hemorrhage	Midbrain and pons	R laterocollis, L rotation	4 months after hemorrhage	Deep tendon reflexes could not be elicited, L hemihypaesthesia	L hemidystonia, oculomotor disturbances, dysarthria, flaccid tetraparesis, ataxia, dysmetria, R postural and kinetic tremor
15	Loher (2009)	56/M	Hemorrhage	L pons, L middle cerebellar peduncle	R laterocollis, L rotation	1 month after hemorrhage	Hypesthesia of L face. R hemihypesthesia	L hemidystonia, blepharospasm, L facial palsy, dysarthria, L hemiataxia. R hemiparesis. Resting, postural and kinetic tremor of all extremities and head
16	Chang (2002)	23/M	Posttraumatic hemorrhage	L GPi	L rotation	3 years after hemorrhage		Mild R hemiparesis, mild dysarthria
17	Zadro (2008)	48/F	Infarct	L cerebellum	R rotation, anterocollis	Second day after hospital admission for vertigo, vomiting.		Ataxia. Horizontal, bidirectional, nystagmus.
18	Usmani (2011)	37/M	Hemorrhage	Vermis/R cerebellum	L rotation	15 months after hemorrhage		R horizontal nystagmus, ataxic gait, dysarthria, R dysmetria and difficulty with finger nose test.

19	O'Rourke (2006)	35/F	Infarct	L and R cerebellum	R rotation	3 days after hospital admission for weakness of legs, vertigo, vomiting, and blindness.		Bilateral blepharospasm, homonymous paracentral scotoma, truncal ataxia
20	Batla (2015)	56/F	Tumor	L cerebellum	R rotation	Information unavailable	Information unavailable	Dysmetria on finger nose test, dystonic tremor
21	Batla (2015)	33/M	Cyst	R cerebellum	R rotation	Information unavailable	Information unavailable	
22	Batla (2015)	58/M	Infarct	L cerebellum	R rotation	Information unavailable	Information unavailable	Dystonic tremor
23	Batla (2015)	29/M	Cyst	L cerebellum	L rotation	Information unavailable	Information unavailable	Dysmetria on finger nose test, dystonic tremor
24	Kirton (2001)	60/F	Infarct	L and R GP	Asymmetric and variable with rotation, antero-, retro-, and laterocollis	Blepharospasm began approximately 2 years after infarction. Dystonia progressed over several years to include oromandibular and cervical dystonia		Meige syndrome, dysmetria and dysdiadokinesia. Slow and wide gait
25	Lambrecq (2010)	23/M	Tumor (ependymoma)	R lateral ventricle, R caudate nucleus, and adjacent white matter	Anterocollis	Acute onset, scan taken within days		Bilateral blepharospasm

Supplementary Table 2. Detailed breakdown of cluster locations
Table 2A: Cerebellar cluster

499 voxels in total. COG at xyz MNI-coordinate 1 -54 -34 in right Lobule IX (vermis)

Voxels	Hemisphere	Location	% of total cluster	% of location intersected
85.2	right	Lobule IX (hemisphere)	17.1	11.9
81.3	left	Lobule IX (hemisphere)	16.3	12.8
35.1	right	Dorsal Dentate Nucleus	7	28.9
33.7	left	Dorsal Dentate Nucleus	6.7	20.6
23.4	left	Lobule IX (vermis)	4.7	26.1
21.7	right	Lobule IX (vermis)	4.4	21.3
11.4	right	Lobule X (vermis)	2.3	64.3
10	left	Lobule X (vermis)	2	73.1
9.8	left	Lobule X (hemisphere)	2	7.7
7.9	left	Interposed Nucleus	1.6	18
6.6	right	Ventral Dentate Nucleus	1.3	14.3
6.4	right	Interposed Nucleus	1.3	17
5.2	left	Fastigii Nucleus	1	11.9
3	right	Lobule X (hemisphere)	0.6	3
1.8	right	Fastigii Nucleus	0.4	6.1
0.8	left	Ventral Dentate Nucleus	0.2	1.5
0.6	left	Lobule VIIIb (hemisphere)	0.1	0.1
0.5	right	Lobule VI (hemisphere)	0.1	0
0.4	left	Lobule VIIIa (vermis)	0.1	0.3
0.3	right	Lobule VIIIb (hemisphere)	0.1	0
0.3	right	Lobule VIIIa (vermis)	0.1	0.1
Total assigned				
345.3			69.2	

Table 2B: Left and right hemisphere somatosensory cortex clusters

548 voxels in total. COG at xyz MNI-coordinate at 45 -24 60 in Brodmann's area 1

Voxels	Hemisphere	Brodmann's area	% of total cluster	% of location intersected
121.4	right	1	22.1	17.2
72.6	right	4a	13.3	6.7
46.4	right	3b	8.5	7.4
13.9	right	2	2.5	2.1
13.1	right	4p	2.4	4.2
Total assigned				
267.4			48.8	

478 voxels in total. COG at xyz MNI-coordinate at -45 -28 59 in Brodmann's area 1

118.2	left	1	24.7	20.7
94.8	left	3b	19.8	16.8
68.1	left	4a	14.3	7.3
44.6	left	2	9.3	8.5
8.1	left	4p	1.7	2.5
Total assigned				
333.9			69.8	

Supplementary Table 3. Abnormal functional connectivity in idiopathic CD patients. Table shows voxels with abnormal connectivity from 'specific' CD ROIs within cerebellum and somatosensory cortex (Figure 5). xyz coordinates of center of gravity of cluster are listed. 'Direction' column shows whether there was significantly greater functional connectivity for cervical dystonia (CD) patients (orange/yellow in Fig.5), or healthy volunteers (HV) (blue/green in Fig.5).

Cerebellum connectivity

Direction	Voxels	x	y	z	P(FWE)	Brain region
>CD	1745	48	-12	30	0.002	R sensorimotor cortex
>CD	72	36	-32	63	0.024	R somatosensory cortex
>CD	71	-43	-22	20	0.024	L central operculum
>CD	46	7	2	63	0.024	R supplementary motor area
>CD	33	-55	-11	12	0.042	L central operculum
>CD	19	-35	-57	-17	0.034	L fusiform gyrus
>CD	10	-34	-60	-11	0.046	L fusiform gyrus
>CD	8	-36	-48	-17	0.046	L temporal/occipital lobe
>CD	6	-37	-2	-5	0.046	L insular cortex
>CD	5	33	-23	60	0.046	R somatosensory cortex
>CD	4	20	-43	-5	0.048	R lingual gyrus
>CD	4	11	-1	52	0.046	R supplementary motor area
>CD	1	66	4	14	0.048	R motor cortex
Somatosensory cortex connectivity						
>CD	461	3	-11	13	0.008	Basal ganglia, thalamus
>CD	95	2	33	20	0.034	Anterior cingulate cortex
>CD	34	-25	1	10	0.04	L putamen
>CD	16	-27	4	0	0.042	L putamen
>CD	7	-26	-15	0	0.049	L globus pallidus
>CD	1	-4	36	14	0.049	Anterior cingulate cortex
>CD	1	4	42	6	0.049	Anterior cingulate cortex
>HV	1486	22	-71	10	0.006	R occipital lobe
>HV	19	-18	-82	42	0.024	L occipital lobe
>HV	14	-23	-46	-5	0.032	L lingual gyrus
>HV	10	48	-6	27	0.038	R sensorimotor cortex

Supplementary Table 4. Control ROI analysis. To assess whether our cerebellar and somatosensory ROIs were specifically abnormal in CD, we compared their seed-based connectivity to 19 control ROIs within our idiopathic CD dataset. Right-most column shows absolute average T-value (comparing idiopathic CD patients to healthy volunteers) from each ROI, to every other voxel within the brain.

	Study	Neurological symptom	ROI brain region	Abs T-value
1	Present study	Cervical dystonia	Somatosensory cortex	0.99
2	Present study	Cervical dystonia	Cerebellum	0.95
3	Boes et al., 2015	Peduncular hallucinosis	L inferior lateral occipital cortex	0.88
4	Laganiere et al., 2016	Hemichorea-hemiballismus	Posterolateral putamen	0.87
5	Boes et al., 2015	Peduncular hallucinosis	Anterior cingulate cortex	0.85
6	Fasano et al., 2016	Freezing of gait	Dorsal medial cerebellum	0.85
7	Joutsa et al., 2018	Parkinsonism	Bilateral claustrum	0.85
8	Boes et al., 2015	Subcortical aphasia	L inferior frontal gyrus	0.83
9	Boes et al., 2015	Central post-stroke pain	R middle temporal gyrus	0.83
10	Darby et al., 2017	Delusional misidentifications	R frontal cortex	0.83
11	Darby et al., 2018b	Free will volition	Anterior cingulate cortex	0.83
12	Darby et al., 2018a	Criminal behavior	Lingual/occipital, intraparietal sulcus	0.83
13	Boes et al., 2015	Subcortical aphasia	L precuneus/white matter	0.82
14	Fischer et al., 2016	Coma	Pregenual Anterior Cingulate Cortex	0.82
15	Darby et al., 2017	Delusional misidentifications	L retrosplenial cortex	0.82
16	Boes et al., 2015	Auditory hallucinosis	L superior temporal gyrus	0.81
17	Boes et al., 2015	Auditory hallucinosis	L fronto-insular cortex	0.80
18	Fischer et al., 2016	Coma	Anterior insula	0.80
19	Boes et al., 2015	Central post-stroke pain	L insula	0.79
20	Darby et al., 2018b	Free will agency	Precuneus	0.79
21	Darby et al., 2018a	Criminal behavior	Ventromedial prefrontal cortex	0.79